Effect of Structure-Soil-Structure Interaction (SSSI) between Three Dissimilar Adjacent Bridges

Mohanad Talal Alfach
City University of London
Ashraf Ayoub (Ashraf.Ayoub.1@city.ac.uk)
City University London https://orcid.org/0000-0002-2670-9662

Research Article

Keywords: SSSI, different superstructure masses, inter-Bridge spacing, geometrical position, nonlinear, seismic, three-dimensional

Posted Date: April 1st, 2021

DOI: https://doi.org/10.21203/rs.3.rs-368849/v1

Abstract

The present study assesses the effect of Structure-Soil-Structure-Interaction (SSSI) on the seismic behavior of three dissimilar adjacent bridges by comparing their seismic responses with the seismic response of the isolated bridge including Soil-Structure-Interaction (SSI). To this end, an extensive series of numerical analyses have been carried out to elicit the effects of Structure-Soil-Structure-Interaction (SSSI) on the seismic behavior of three dissimilar bridges with different superstructure masses. The studied bridges are based on groups of piles founded in nonlinear clay. A parametric study has been performed for configurations of three dissimilar bridges with superstructure masses ratios of 200% and 300%, concentrating on the influence of the inter-bridge spacing, and the geometrical position of the bridges towards each other and towards the seismic excitation direction. The numerical analyses have been conducted using a three-dimensional finite difference modeling software FLAC 3D (Fast Lagrangian analysis of continua in 3 dimensions). The results of the numerical simulations clearly show that the seismic responses of the dissimilar grouped bridges were strongly influenced by the neighboring bridges. In particular, the results reveal a salient positive impact on the acceleration of the superstructure by a considerable drop (up to 90.63%) and by (up to 91.27%) for the internal forces induced in the piles. Comparably, the influence of bridge arrangement towards the seismic loading were prominent on both of superstructure acceleration and the internal forces in the piles. The responses were as much as 27 times lesser for the acceleration and 11 times smaller for the internal forces than the response of the isolated bridge. Contrarily, the inter-bridge spacing has a limited effect on the seismic response of the grouped bridges.

1. Introduction

As most structures in densely populated urban areas are constructed in clusters, and often with only a few meters apart, their seismic response is thoroughly affected by the dynamic behavior of the adjacent structures and their fundamental dynamic characteristics; this interaction is termed as Structure-Soil-Structure Interaction (SSSI). Whence, the study of (SSSI) effects has become increasingly inevitable to ensure an effective earthquake resilience of the structures constructed in dense urban environments. Furthermore, the accelerated lack of available space has led in some cases to construct new large structures near old smaller structures in new neighborhoods which impose additional complications to the (SSSI) effects. The state-of-the-art in (SSSI) analysis has been mostly concentrated on tall buildings and skyscrapers; the effect between neighboring bridges have been rarely studied, mainly due to the shortage of experimental or field-based case-studies that confirm its effect on seismic response. The numerical analyses presented herein share the common goal of a better understanding of the phenomena of (SSSI), with particular attention to focusing on the effect of (SSSI) between three dissimilar adjacent bridges, different superstructure mass ratios, inter-bridge spacing, and the arrangement of the bridge towards the seismic loading direction.

Structure-Soil-Structure-Interaction (SSSI) has attracted extensive attention in the last decades; most prior research about (SSSI) have generally concentrated on the seismic behavior of neighboring tall buildings and skyscrapers. Nevertheless, there is rather a variance between the findings of these studies in the literature. In the numerical field, Kim (2014) has employed a three-dimensional (3D) Finite Element model to analyze the seismic interaction between three connectors and the surrounding soil at different bridge superstructure elevations of an existing bridge interchange at the intersection of Interstates 10 and 215 (San Bernardino, CA). Bolisetti and Whittaker (2015) have performed a series of numerical simulations and centrifuge experiments to assess the seismic effects of (SSSI) on buildings constructed in dense urban environments. They have asserted that the experiments and numerical results have revealed a slight effect of (SSSI) on the seismic response of the buildings considered in their research. Lu et al. (2020) have developed simple discrete models for simulating the static and dynamic interaction between multiple buildings. The developed models have been validated by comparison with the results of the simulation methods of Finite elements (FE) and Boundary elements (BE). A thorough series of 2D numerical analyses have been carried out by Bybordiani and Arici (2019) to study the interaction effect between neighboring 5-, 15-, and 30-story clusters of structures and the surrounding viscoelastic half-space. They have investigated the influence of the inter-building distance and the foundation material on the response of the adjacent buildings. The

results have revealed negligible effects of (SSSI) on the behavior of the identical low-rise structures and significant effects on the response of the identical high-rise structures. In the same manner, Isbiliroglu et al (2015) have conducted parametric numerical analyses to study the effects of (SSSI) for various arrangements of regular building clusters composed of three types of buildings of approximately 3, 13, and 40 stories. The results pointed out to considerable drop in buildings base motion at frequencies above the natural frequencies of the building-foundation systems. Likewise, both detailed numerical analyses and a set of centrifuge experiments have been employed by Bolisetti and Whittaker (2020) in order to investigate the effect of (SSSI) on three arrangements of low- to medium-rise frame buildings. They concluded that the existence of deep vault reduces uplift in the foundations and the peak spectral accelerations at the roof. Ogut (2017) has conducted a wide (SSSI) analytical parametric study; the effects of mass, height of the superstructures, foundation types, embedment situations and fixed based natural frequencies of two and three closely spaced buildings on (SSSI) have been investigated. By studying the (SSSI) effect on 32 story neighboring buildings for different inter-building spacing, Yahyai et al. (2008) have claimed a detrimental effect of (SSSI) on base shear forces and lateral displacement. As well as detailed numerical analyses for obliquely incident seismic waves have been carried out by Álamo et al. (2015). They noted that the inter-building spacing and the seismic loading are crucial for the (SSSI) effects on short identical structures supported by pile foundations. In a related study, Rahgozar (2015) has employed the direct method for evaluating the behavior of three-dimensional finite element models of neighboring 15 and 30 story steel structures founded on different sandy and clayey soils. The results demonstrated the detrimental effect of (SSSI) for the case of neighboring tall buildings to short buildings. Nakamura et al. (2012) have conducted a comprehensive seismic analysis by using a nonlinear three-dimensional FEM model to determine the (SSSI), and the ground irregularity effect on the seismic response of NPPs (Nuclear Power Plants). Roy et al. (2015) have performed a detailed parametric study to analyze the impact of (SSSI) on the behavior of neighboring light structure to a heavy structure, and a heavy structure adjacent to a heavy structure for several soil cases, foundation embedment depths, and separation distances. The results asserted that the SSSI response of light or heavy structures can be influenced by the existence of a nearby heavy structures. Barrios and Chouw (2015) have performed a physical experimental study by using a sand-filled laminar box on a shaking table. The examined adjacent structures had identical mass and different fundamental periods. They concluded that the buildings with lower natural frequencies are less vulnerable to the (SSSI) effect than the buildings with higher natural frequencies. Ikeda et al. (2004) have conducted a comprehensive analytical and numerical study on the (SSSI) effect among multiple foundations (without superstructures). Larkin et al. (2016) have performed shaking table tests with a laminar box for 4 neighboring buildings. They denoted that the (SSSI) effect are more evident for neighboring structures with different fundamental frequencies due to the mechanism of energy exchange between them. Ge et al. (2017) have conducted comprehensive experimental tests and numerical studies to investigate the (SSSI) effect between multiple high-rise buildings. The results revealed beneficial effect of the (SSSI) on the acceleration responses of structures and adverse effect on the structures deformations. Furthermore, two centrifuge tests have been performed by Trombetta et al. (2014) to assess the (SSSI) effects between midrise elastic shear-wall buildings supported by a mat foundation and low-rise inelastic frame buildings built on individual spread footings. Andersen et al (2017) have extended the validity of a semi-analytical model predicting ground vibration from rigid rectangular loads to enable it of estimate accurately the effect of heavy masses or plates set either on the ground surface or implanted into the soil. Similarly, Gan et al. (2020) carried out a thorough numerical analyses of the (SSSI) effect between three adjacent structures supported by pile-raft foundations embedded in viscoelastic half-space. The results revealed that the (SSSI) impact depends mainly on the structural characteristics, rather than the location of the structures. Wang (2018) has employed the finite element software (ANSYS) to analyze the (SSSI) effect between surface structure built on viscous-elastic soil layer and the adjacent underground station. The results denoted that the arrangement and the fundamental frequencies of the structures have the crucial impact on the (SSSI) effect. Bard et al (2013) have conducted extensive experimental, numerical and theoretical cross-analysis to quantify multi-building interactions (SSSI) and site-city effect. An idealized experimental model of a city on a soft layer has been used to examine the effect of multiple Structure-Soil-Structure interactions (SSSI). Schwan et al. (2016) have performed a set of shake table tests on a designed elementary case study of multiple (SSSIs) between clusters of structures. The experimental data were compared with theoretical and numerical results. They demonstrated experimentally, theoretically, and numerically the fact that a city group effect can

significantly alter the seismic response of both the construction site and the related buildings; also, they quantified the complex (SSSIs) at the city scale. Mason et al. (2010) have conducted centrifuge tests on two adjacent moment-resisting-frame steel structures. The first model structure is a one-story, lumped-mass frame structure based on embedded spread footings. The other model structure is a three-story, lumped-mass frame structure founded on a one-story aluminum basement. A comprehensive set of dynamic geotechnical centrifuge tests has been carried out by Ngo at al. (2019) to investigate (SSSI) effects on the behavior of two adjacent structures with different mass, natural frequency, and height. Extensive numerical analyses have been implemented by Alam and Kim (2014) to explore the effect of uniform and non-uniform ground motions on the behavior of neighboring reinforced concrete (RC) frame structures. The results revealed a remarkable impact of the spatial variation of ground motions on the seismic response of the adjacent structures. Ritter (2017) has employed at novel three-dimensional technology to investigate the (SSSI) effect between a tunnel, the soil, and existing structures. The building models were printed with brittle material behaviour similar to masonry and tested in a geotechnical centrifuge. A thorough series of numerical analyses have been conducted by Alfach and Al Helwani (2019) to examine the effect of the plan positioning of the bridges towards the seismic excitation direction and inter-bridge spacing for two identical bridges supported by a group of piles embedded in nonlinear clay. Knappett et al. (2015) have examined the seismic performance of an isolated structure and adjacent (similar and dissimilar) structures under a series of strong seismic excitations. The non-linear dynamic centrifuge tests were accurately validated by a comprehensive non-linear finite-element model. Furthermore, Ada et al. (2019) have investigated the (SSSI) effect between two neighbouring frame structures through a series of 3D numerical analysis. They have examined the influences of the stiffness of the underlying soil, layout of the structures, the clear distance between the structures, and the number of stories of the structures. They concluded the (SSSI) effect highly depended on the dynamic characteristics of the adjacent structures.

1.1 Aims

The main objective of this paper is developing better understanding of the seismic structure-soil-structure interaction (SSSI) between three dissimilar bridges with different superstructure mass ratios. Notably, the contents of this study focused on the effect of inter-bridge spacing and dissimilar bridge geometrical arrangements on the (SSSI) impact. In this paper, we enlarge the range of our former studies about the (SSSI) effect between two identical bridges in Alfach and Al Helwani (2019), and the (SSSI) effect between two dissimilar bridges in Alfach (2021) to study the case of three dissimilar bridges with different superstructure mass ratios. The numerical analyses were performed using a finite-difference modeling software FLAC 3D (Fast Lagrangian analysis of continua in 3 dimensions). The analyses have been undertaken for non-linear clay.

More Specifically, the research contributions in assessing the effect of the seismic structure-soil-structure- interaction (SSSI) could be summarized in these three points:

- Identification of the nature of (SSSI) effect (detrimental, constructive, or neutral) between three adjacent dissimilar bridges with different superstructure ratios.

- Explore the impact of inter-bridge spacing on the seismic performance of the neighboring bridges.

- Investigation of the seismic efficiency of the planned alignment of adjacent structures with respect to each other and the epicentral direction (Parallel, Perpendicular, Crossing).

2. Numerical Model Of Adjacent Bridges

2.1 *Soil-pile-bridge model*

The (SSSI) system in this study consisted of three asymmetric reinforced concrete bridges. These bridges of lumped masses of (350, 700, and 1050 Tons) have been used for forming different neighborhood combinations. The used bridges were supported by floating piles groups of (6, 12, and 18 piles) respectively, for the purpose of retaining the single pile static

axial load to (80 tons). The fixed-head pile groups are embedded into homogeneous nonlinear cohesive layer (C=150 KPa, □ = 0) underlined by rigid bedrock as shown in (Figure 2). The soil behavior was simulated based upon the standard Mohr-Coulomb criterion through an elastoplastic law without hardening. Table (1) presents the essential geotechnical characteristics of the soil layer. The length and the diameter of the piles are (L_p = 10.5 m) and (D_p = 0.8 m) respectively. The piles are connected rigidly by a reinforced concrete cap of (1 m) thick as illustrated in figure (1). The comportment of the material of the structural elements (superstructure mass, bridge pillar, cap, and piles) has been defined as elastic. Tables (2) and (3) lists the fundamental parameters of the superstructure and the pile groups, respectively.

Table 1. Properties of cohesive soil.

ρ_s (Kg/m^3)	E_{os} (MPa)	□s	K_o	ζ_s (%)	C (Kpa)	□ (0)	Ψ (0)
1700	8	0.3	0.5	5	150	0	0

Table 2. Elastic characteristics of the Superstructure

ρ_{st} (Kg/m^3)	E_{st} (MPa)	v_{st}	ξ_{st} (%)	Masse (Tons)
2500	8000	0.3	2	350

Where ρ_{st}, E_{st} and v_{st} are the density, young's modulus and the coefficient of Poisson's ratio. ξ_{st}: is the percentage of critical damping. D_p: is the pile diameter. E*A and E*I are the axial and bending stiffness.

Table 3. Elastic characteristics of the Piles materials

Material	Diameter (m)	Mass Density ρ(Kg/m^3)	Young Modulus E (MPa)	Poisson ratio v	Damping ratio ξ (%)	Height (m)
Pile	0.8	2500	20000	0.3	2	10

In light of the high complexity of the subject of Structure-Soil-Structure Interaction (SSSI), a set of measures have been adopted:

- Aiming to minimize the computational cost, the soil mesh density was decreased with increase of the distance from the soil center, where the major effect of (SSSI) could be taken place as shown in figure (2).

- The absorbent boundaries have been employed to avoid the seismic wave's reflection on the structures model zone.

- In order to prevent the potential soil-cap interaction, the cap was based a 0.5 m over the soil surface.

- In order to preclude the possible pile-pile interaction, the inter-piles distance was taken as (S =3.75D_p =3 m).

To reduce the computation cost, the superstructure was simulated by lumped masses at the top of the pillars [M_{st}=350, 700, 1050 Tons] respectively. The flexural stiffness of the superstructure is [K_{st} = 86840, 1389440, 1389440 KN/m] respectively,

and its fundamental frequencies (assuming a fixed base) are equal to [F_{st}=2.5, 7.09, 5.78 Hz] respectively. The latter were computed by using the subsequent formulations:

$$f_{st} = \frac{1}{2\Pi}\sqrt{\frac{K_{st}}{M_{st}}}\ , \qquad K_{st} = \frac{3EI_{st}}{H_{st}^3} \quad (1)$$

While the fundamental frequency of the soil layer is 3.2 Hz. The flexible base frequencies of the superstructure taking into consideration the soil-structure interaction were calculated (using numerical methods) as $F_{st,flex}$= 0.827, 0.71, and 0.7 Hz respectively.

2.2 Seismic excitation

The numerical analyses have been carried out under the seismic record of the Kocaeli Earthquake (Mw = 7.4) which occurred on August 17, 1999, in the North Anatolian Fault Zone in Turkey (Station AMBARLI; KOERI source). The peak horizontal acceleration and velocity of this earthquake are (PGA =0.247 g) and (PVA =40 Cm/s) respectively during the total duration of the record (t = 30.08 Sec). Nevertheless, the numerical analyses have been performed for a duration of (t=8.465 sec) to economize the computational capacity and the analyses durations. This step was adopted after rigorous analysis to ensure the equalization of the seismic excitation impact for the total duration (t = 30.08 sec) and the used duration (t=8.465 sec). Figure (3) presents the fundamental frequency of the seismic loading (F= 0.9 Hz) in the Fourier spectrum of the velocity record (figure 3D). It is worth mentioning that the seismic loading fundamental frequency is between the fundamental frequency of the soil (F_1 = 3.2 Hz) and the flexible frequency of the structure (F_{ss} = 0.7 Hz) which justifies the choice of this seismic loading.

2.3 Results and Discussion

Table 4 and figures (4) and (5) introduce the results of the bridge with superstructure mass of (M_{st}= 350 T). The results exhibit an important amplification factor at the superstructure mass (A_{amp} =10.8). Furthermore, it is worth noting that the maximal internal forces occurred in the upper and central parts of the piles.

Table 4. response of a group of (2*3) piles for Kocaeli earthquake (1999).

C Cohesion (KPa)	a_{st} (m/s²)	a_{Cap} (m/s²)	Internal forces			
			Central piles		Corner Piles	
			M_{max} Bending Moment (KN.m)	T_{max} Shear Force (KN)	M_{max} Bending Moment (KN.m)	T_{max} Shear Force (KN)
150	23.02	14.39	2244	1218	2189	1604

As shown in figures (6) and (7) and table 5, the maximum internal forces induced in the piles of the bridge of (M_{st}= 700 T) are smaller by about (25 %) than those of the piles of the bridge of (M_{st}= 350 T). Furthermore, the amplification factor at the mass was reduced by a ratio of (A_{amp} =7.95). Also, it is noteworthy that the bending moment profile has changed drastically by recording the maximum values at the top parts of the piles.

Table 5. response of a group of (4*3) piles for Kocaeli earthquake (1999).

C (KPa)	a_{st} (m/s²)	a_{Cap} (m/s²)	Internal forces			
			Central piles		Corner Piles	
			M_{max} (KN.m)	T_{max} (KN)	M_{max} (KN.m)	T_{max} (KN)
150	18.09	14.9	1411	837.8	1732	1233

Finally, the maximum bending moment (M= 2947 KN.m) and the minimum shear force (T= 623.3 KN) among the three isolated bridges of superstructure masses (M_{st}= 350, 700, 1050 T) were obtained for the bridge of mass (M_{st}= 1050 T) as shown in figures (8) and (9). Additionally, the mass and cap accelerations of the bridge of mass (M_{st}= 1050 T) have dropped sensibly to (11.99) and (10.82) respectively as presented in table (6). Likewise, the amplification factor of the mass has decreased to (A_{amp}= 5.64).

Table 6. response of a group of (6*3) piles for Kocaeli earthquake (1999).

C (KPa)	a_{st} (m/s²)	a_{Cap} (m/s²)	Internal forces			
			Central piles		Corner Piles	
			M_{max} (KN.m)	T_{max} (KN)	M_{max} (KN.m)	T_{max} (KN)
150	11.99	10.82	2363	623.3	2947	1007

3. Bridge-soil-bridge System

The following numerical simulations have been carried out for several configurations of three dissimilar bridges for two superstructure mass ratios (200 % and 300 %). The impact of two essential factors have been examined: 1) Inter-bridge spacing and, 2) The geometric position of neighboring structures towards each other and the seismic loading direction (Parallel, Perpendicular, Crossing) configurations for the above-stated mass ratios.

3.1 Three bridges with superstructure mass ratio (200 %)

3.1.1 Effect of Inter-Bridge spacing

The effect of the inter-bridge spacing on the (SSSI) effect between three different parallel bridges has been numerically analyzed; the central bridge is the heavier one with a superstructure mass of (M_{st}=700 T) (figure 2.b) located between two lighter bridges with a superstructure mass of (M_{st}= 350 T) (figure 2.a). The numerical calculations were undertaken for a range of distances between the bridges, precisely (S= 20 m,30, and 40 m). All the geometrical and mechanical characteristics of soil and concrete mentioned in section (2.1) and tables (1,2, and 3) have been adopted in these analyses. The numerical simulation is performed for the seismic loading of the Turkey earthquake (Kocaeli,1999). The applied mesh presented in figure (10) includes (4176) zones of 8 node solid elements and (552) three-dimensional structural elements of 2 node beam elements.

3.1.1.1 Results and Discussion

The spread of the plasticity in the soil for the two isolated bridges (M_{st} =350 and 700 T) are presented in figure (10). Foreseeably, the plasticity extension under the central part of the light bridge (M_{st}= 350 T) is much smaller than its peer

under the heavy bridge. Likewise, figure (11) illustrates the plasticity extension for the inter-bridge spacing (S= 20,30, and 40 m) between three parallel dissimilar bridges under the effect of seismic loading (Kocaeli, 1999).

The plasticity spread in the soil has slightly reduced with the increase of the inter-bridge spacing as shown in figure (11). On the other hand, the plasticity has dominated the comportment of the upper part of the soil (C= 150 KPa), whilst the behavior of the lower part stayed mostly elastic due to the fact that the plasticity has started at the soil surface and extended gradually towards the base without attaining the base during the seismic loading time.

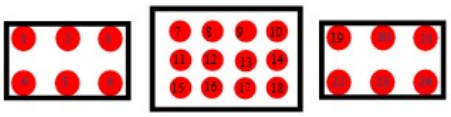

Table 7 Influence of the spacing inter-bridge on the seismic response of three dissimilar parallel bridges system

S (m)	a_{st} (m/s²)	a_{Cap} (m/s²)	Internal forces							
			Central piles				Corner Piles			
			Pile (2) (M_{st}=350 T)		Pile (16) (M_{st}=700 T)		Pile (1) (M_{st}=350 T)		Pile (7) (M_{st}=700 T)	
			M_{max} (KN.m)	T_{max} (KN)	M_{max} (KN.m)	T_{max} (KN)	M_{max} (KN.m)	T_{max} (KN)	M_{max} (KN.m)	T_{max} (KN)
One Bridge (M_{st}=350 T and S=0)	**23.02**	**14.39**	**2244**	**1218**			**2189**	**1604**		
One Bridge (M_{st}=700 T and S=0)	**18.09**	**14.9**			**1640**	**1134**			**1732**	**1233**

S (m)	Bridge (M_{st}=350 T)		Bridge (M_{st}=700 T)		Three dissimilar parallel bridges							
					Pile (2)		Pile (16)		Pile (1)		Pile (7)	
	a_{st}	a_{Cap}	a_{st}	a_{Cap}	(M_{st}=350 T)		(M_{st}=700 T)		(M_{st}=350 T)		(M_{st}=700 T)	
20	**11.5**	**6.61**	**8.45**	**5.78**	**1981**	**1169**	**1123**	**998**	**1824**	**1310**	**1218**	**1090**
30	**11.8**	**6.88**	**8.63**	**5.94**	**2021**	**1200**	**1156**	**1006**	**1870**	**1273**	**1222**	**1118**
40	**12**	**7.1**	**8.81**	**6.05**	**2035**	**1242**	**1176**	**1037**	**1935**	**1361**	**1278**	**1157**

Table. 7 indicates an important positive effect of the (SSSI) on both of the superstructure acceleration and the internal forces induced in the piles. The mass acceleration of the light bridge (M_{st}= 350 T) drops sharply (up to 53.28 %) due to the (SSSI) effect; similarly, the mass acceleration of the heavy bridge (M_{st}= 700 T) decreases by (up to 50 %). In the same manner, the cap acceleration of the heavy bridge (M_{st}= 700 T) and the light bridge (M_{st}= 350 T) reduces by (up to 61.2 %, and 54 %) respectively. Regarding the impact of (SSSI) on the internal forces induced in the piles, the bending moment and the shear force induced in the piles of the heavy bridge (M_{st}= 700 T) reduced by (up to 31.5 % and 12 %) respectively as illustrated in figures (12) and (13). Similarly, Figures (14) and (15) show a comparable effect of the (SSSI) on the piles of the light bridge (M_{st}= 350 T) via decreasing the bending moment and the shear force by (up to 16.6 % and 20.6 %) respectively. Hence, the interaction between three dissimilar bridges (SSSI) has valuable positive impacts on the

superstructure acceleration and the piles internal forces by provoking a significant diminution of both. Table 7 and Figures 12, 13, 14, and 15 demonstrate the slight influence of the inter-bridge spacing on the internal forces provoked in the piles of the three bridges, which are in accord with the results of Alfach and Al Helwani (2019) and the results of Alfach (2021) about the minor impact of the inter-bridge spacing. Substantially, the bending moment and the shear force induced in the piles of the light bridge (M_{st}= 350 T) increase by (up to 6 % and 6.9 %) respectively with the rise of the inter-bridge spacing. Likewise, the bending moment and the shear force of the heavy bridge (M_{st}= 700 T) augment by (up to 4.9 % and 6.1 %) respectively. In the same manner, the mass and the cap accelerations increase by (up to 4.3 % and 7.41 %) respectively with the increase of the inter-bridge spacing as revealed in figure (16). It is worth mentioning that all the maximum internal forces induced in the piles have been obtained in the heads of the piles except the maximum bending moment induced in the piles of the bridge of (M_{st}= 350 T), which has been obtained in the central part of the piles as seen in figures (14) and (15).

In the frequency domain, figure (17a) compares the three dominant frequencies of the mass of the heavy bridge of (M_{st}= 700 T) for the configuration of three adjacent bridges for three inter-bridge spacing (S=20, 30, and 40 m) with the dominant frequency of the isolated one bridge of (M_{st}= 700 T). The dominant frequency peak (F= 0.732 Hz) of the isolated one bridge of (M_{st}= 700 T) drops to (F= 0.7 Hz) for the configuration of three neighboring bridges. Likewise, for the light bridge (M_{st}= 350 T), figure (17b) shows that the dominant frequency decreases from (F= 0.709 Hz) for the isolated one bridge to (F= 0.6 Hz) for the case of adjacent three bridges for the three aforementioned inter-bridge spacing.

3.1.2 Effect of bridge plan alignment with respect to each other and the seismic loading direction

Three combinations of bridges with respect to the direction of seismic excitations composed of three dissimilar (parallel, Perpendicular, and Crossing at 45^{o}) have been considered for the above-mentioned heavy bridge of (M_{st} = 700 T) and light bridge of (M_{st} = 350 T). An extensive series of numerical calculations were carried out on the three mentioned configurations of (parallel, Perpendicular, and Crossing) bridges to evaluate the influence of the direction of the bridges towards each other and towards the seismic loading direction on the (SSSI) effects. The numerical analyses were performed for inter-bridge spacing of (S= 20 m) and under the seismic record of Turkey (Kocaeli,1999) presented in figure (3). Furthermore, the mechanical and geometrical properties demonstrated in figure (1) and tables (1), (2), and (3) have been used in these calculations. The adopted mesh for perpendicular and crossing configurations displayed in figures (18) and (19) respectively includes (77990) nodes and (552) beam structural elements of 2 nodes.

3.1.2.1 Results and discussion

Figure (20) demonstrates the deep extension of the plasticity under the perpendicular isolated bridge of (M_{st} = 350 T); differently the plasticity prolongation was substantially smaller for the heavy isolated bridge (M_{st} = 700 T). Similarly, the plasticity zones under the light bridges of (M_{st} = 350 T) and the heavy bridge of (M_{st} = 700 T) reduced significantly for the perpendicular and crossing configurations. Nevertheless, the plasticity has prolonged and attained the soil base under the heavy bridge of (M_{st} = 700 T) for the crossing bridges' configuration.

Table 8 and figures (22 to 26) demonstrate the key constructive role of the (SSSI) on the seismic behavior of the neighboring bridges. Both the superstructure acceleration and the piles internal force reduced significantly under the crucial impact of the (SSSI). Concerning the acceleration of the superstructure, the mass and cap accelerations of the light bridge of (M_{st} = 350 T) have decreased considerably (up to 42.8 %) and (up to 42.5 %) respectively. Correspondingly, the mass and cap accelerations of the heavy bridge of (M_{st} = 700 T) have reduced drastically by (up to 58.8 %) and (up to 53.72 %) respectively. The beneficial impact of the (SSSI) on the piles internal forces was much pronounced through very large reduction of the bending moment and the shear force of the light bridge of (M_{st} = 350 T) by (up to 88.49 %) and (up to 88.7 %) respectively. Similarly, but by smaller ratios the bending moment and the shear force of the heavy bridge (M_{st} = 700 T) have dropped by (up to 44.53 %) and (up to 74.2 %) respectively.

Table 8 Influence of different positioning of three dissimilar bridges on the seismic response system

Position	a_{st} (m/s²)	a_{Cap} (m/s²)	Internal forces							
			Central piles				Corner Piles			
			Pile (2) **(M_{st}=350 T)**		Pile (15) **(M_{st}=700 T)**		Pile (1) **(M_{st}=350 T)**		Pile (7) **(M_{st}=700 T)**	
			M_{max} (KN.m)	T_{max} (KN)	M_{max} (KN.m)	T_{max} (KN)	M_{max} (KN.m)	T_{max} (KN)	M_{max} (KN.m)	T_{max} (KN)
One Perpendicular Bridge (M_{st}=350 T)	**20.1**	**11.5**	**3979**	**1268**			**4093**	**1330**		
One Perpendicular Bridge (M_{st}=700 T)	**20.53**	**12.49**			**2196**	**1325**			**2061**	**1294**

Position	Bridge **(M_{st}=350 T)**		Bridge **(M_{st}=700 T)**		Three dissimilar bridges							
					Pile (2)		Pile (15)		Pile (1)		Pile (7)	
	a_{st}	**a_{Cap}**	**a_{st}**	**a_{Cap}**	**(M_{st}=350 T)**		**(M_{st}=700 T)**		**(M_{st}=350 T)**		**(M_{st}=700 T)**	
Parallel	**11.5**	**6.61**	**8.45**	**5.78**	**1981**	**1169**	**1218**	**1090**	**1890**	**1309**	**1218**	**1090**
Perpendicular	**0.54**	**6.52**	**1.83**	**1.44**	**501.9**	**155.4**	**1508**	**363.1**	**490.4**	**161.2**	**1438**	**328.6**
Crossing	**0.53**	**6.47**	**2.46**	**1.34**	**457.8**	**143.2**	**1367**	**545**	**478.7**	**159.6**	**1367**	**545.2**

In terms of the pile's internal forces, the minimum bending moments induced in the piles (1) and (2) of the light bridge of (M_{st} =350 T) were reported in the configuration of crossing bridges with (M_{min1}= 478.7 KN.m) and (M_{min2}=457.8 KN.m) accompanied with the minimum shear forces (T_{min1}= 159.6 KN) and (T_{min2} =143.2 KN) as revealed in figures (24) and (25). Moreover, the internal forces induced in piles (1) and (2) were very close for the configurations of perpendicular and crossing bridges as provided in table 8 and figures (24) and (25). Conversely, the maximum bending moment and shear force induced in piles (7) and (15) of the heavy bridge (M_{st}=700 T) were reported for the perpendicular bridge configuration. However, the minimum bending moment and shear force in the piles (7) and (15) were noted in the case of parallel bridges as shown in figures (22) and (23). It is noteworthy that the minimum accelerations in the superstructure elements (mass (A_{st}= 0.53 m/sec^2), and cap (A_{cap}=6.47 m/sec^2)) have been observed in the case of crossing bridge configuration for the light bridge of (M_{st}= 350 T) as depicted in figure (26).

Similarly, the best impact of the (SSSI) on the cap acceleration was noted for the minimum cap acceleration of the heavy bridge of (M_{st}= 700 T) which has attained (A_{cap}= 1.34 m/sec^2) for the configuration of the crossing bridges, which agrees with the conclusions obtained by Alfach and Al Helwani (2019) and Alfach (2021). Howbeit, the minimum acceleration in

the mass of the heavy bridge of (M_{st} = 700 T) has been obtained for the perpendicular configuration with (A_{st}= 1.83 m/sec^2) as shown in figure (26a). It is pertinent to note, the perpendicular and crossing configurations have an uncommon impact on the vibration of the superstructure of the light bridge of (M_{st}= 350 T) which was represented by generating the bigger accelerations in the cap by (A_{cap} =6.52, and 6.47 m/sec^2) accompanied with much smaller accelerations in the mass (A_{st}= 0.54, and 0.53 m/sec^2). Figure (27a) shows the spectrum Fourier analyses for the lateral seismic responses of the superstructure mass of the heavy bridge of (M_{st}= 700 T) for the three studied configurations (parallel, perpendicular, and crossing) bridges. The maximum dominant frequency (F=0.7 Hz) was obtained for the parallel bridge configuration; while the dominant frequencies of the crossing and perpendicular bridges configurations were (0.473, and 0.4 Hz) respectively, with much smaller amplitudes. Conversely, for the light bridge of (M_{st}=350 T), the maximum dominant frequency (F= 0.709 Hz) was attained for the crossing bridge configuration with a slight amplitude, while the dominant frequency of the perpendicular bridges is (F= 0.7 Hz) and the dominant frequency of the parallel bridges is (F= 0.6 Hz) with much bigger amplitude as illustrated in figure (27b).

3.2 Two bridges with superstructure mass ratio (300 %)

3.2.1 Effect of Inter-Bridge spacing

A set of numerical analyses have been carried out to examine the influence of inter-bridge spacing on the (SSSI) effect between three different parallel bridges with superstructure masses ratio of (300 %). The same geometrical and mechanical characteristics mentioned in section (2.1) for the light bridge of (M_{st}= 350 T) as shown in figure (2.a) and the heavy bridge of (M_{st}= 1050 T) as presented in figure (2.c) have been adopted. The numerical study has been performed under the velocity record of the Turkey earthquake (Kocaeli,1999) and for a range of inter-bridge spacing precisely (S = 20 m, 30 m, and 40 m). Figure (28) reveals the three-dimensional meshed model used in the analyses.

3.2.2.1 Results and discussion

Predictably, the soil plasticity under the isolated heavy bridge of (M_{st}= 1050 T) has been prolonged deeper than the one under the isolated light bridge of (M_{st} = 350 T), except under the cap limits of the light bridge in the x-direction, where the plasticity extended to about two-thirds of the soil depth. However, the (SSSI) effect resulting from the interaction between the three dissimilar bridges have considerably changed the plasticity extension under the three bridges as illustrated in figure (30). The plasticity prolongation in the zones under the light bridges of (M_{st} = 350 T) is much deeper than the one under the central heavy bridge of (M_{st} = 1050 T). Furthermore, figure (30) reflects the negligible impact of the inter-bridge spacing on the plasticizing of the soil. Furthermore, figure (30) reflects the negligible impact of the inter-bridge spacing on the plasticizing of the soil. Table (9) reveals the valuable effect of the (SSSI) on both acceleration of the superstructure and the internal forces induced in the piles. In further detail, the mass accelerations of the heavy bridge of (M_{st} = 1050 T) and the light bridge of (M_{st} = 350 T) have dropped sharply by (71.8 %) and (42.28 %) respectively. Similarly, the bending moment induced in the piles of the heavy bridge (M_{st} = 1050 T) and the light bridge (M_{st} = 350 T) have decreased considerably by (42.6 %) and (52.8 %). In a similar manner, the shear force induced in the piles of the heavy bridge has significantly reduced by (77.7 %) and by a much inferior ratio for the piles of the light bridge (7 %). A slight effect of the inter-bridge spacing was highlighted in table 9 and figures (31a to 34a). More precisely, the bending moment provoked in the piles of the heavy and light bridges has increased by (10.47 %) and (7.17 %) respectively with the inter-bridge spacing rise. Alike, the shear force induced in the piles of the heavy and light bridges has grown by (7.2 %) and (14.38 %) with the augmentation of the inter-bridge spacing as shown in figures (31b to 34b). It must be mentioned that all the maximum internal forces induced in the piles have been reported in the top of the piles, except the maximum shear force in the piles of the light bridge, which has been obtained in the central part of the piles.

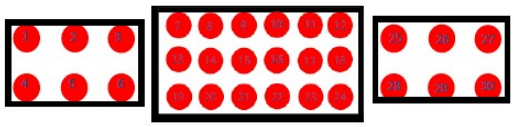

Table 9 Influence of the spacing inter-bridge on the seismic response of Three dissimilar parallel bridges system

S (m)	a_{st} (m/s²)	a_{Cap} (m/s²)	Internal forces							
			Central piles				Corner Piles			
			Pile (2) (M_{st}=350 T)		Pile (15) (M_{st}=1050 T)		Pile (1) (M_{st}=350 T)		Pile (7) (M_{st}=1050 T)	
			M_{max} (KN.m)	T_{max} (KN)	M_{max} (KN.m)	T_{max} (KN)	M_{max} (KN.m)	T_{max} (KN)	M_{max} (KN.m)	T_{max} (KN)
One Bridge (M_{st}=350 T and S= 0)	**20.1**	**11.5**	**3979**	**1268**			**4093**	**1330**		
One Bridge (M_{st}=1050 T and S= 0)	**20.53**	**12.49**			**2196**	**1325**			**2061**	**1294**

S (m)	Bridge (M_{st}=350 T)		Bridge (M_{st}=1050 T)		Three dissimilar bridges							
					Pile (2)		Pile (15)		Pile (1)		Pile (7)	
	a_{st}	a_{Cap}	a_{st}	a_{Cap}	(M_{st}=350 T)		(M_{st}=1050 T)		(M_{st}=350 T)		(M_{st}=1050 T)	
20 m	**11.6**	**11.6**	**5.78**	**4.58**	**2091**	**1189**	**1260**	**294.8**	**1929**	**1236**	**1496**	**426.3**
30 m	**12.1**	**12.2**	**5.95**	**4.79**	**2166**	**1271**	**1322**	**305.4**	**1969**	**1283**	**1517**	**428**
40 m	**12.7**	**12.7**	**6.15**	**5.12**	**2241**	**1360**	**1392**	**316**	**2017**	**1333**	**1552**	**433**

Similarly, the shear force induced in the corner piles of the bridge (M_{st}= 350 T) decreased by (4.96 %) with the increase of the inter-bridge spacing as described in figure (33b). In contrast, the bending moment in the corner piles and the internal forces (bending moment and shear force) in the central piles of the bridge of (M_{st}= 350 T) varies marginally (up to 11 %) without showing an evident trend as illustrated in table 9 and figures (33) and (34). It is worth noting that the maximum bending induced in the piles of the bridge of (M_{st}= 350 T) have been reported in the central part of the piles according to figures (33a) and (34a), while all the other internal forces were obtained in the heads of the pile as depicted in figures (33b) and (34b).

Spectral velocity analyses of Fourier presented in figure (36) exhibit a negligible effect of the inter-bridge spacing on the dominant frequencies for the studied spacing of (S=20, 30, and 40 m) between the three bridges. Almost the dominant frequency is constant (F= 0.827 Hz) for the heavy bridge of (M_{st} = 1050 T) and (F= 0.709 Hz) for the light bridge of (M_{st} = 350 T).

3.2.2 Effect of bridge plan alignment with respect to each other and the seismic loading direction

Two additional numerical analyses have been carried out to examine the effect of the Perpendicular and Crossing bridges configurations on the overall effect of the (SSSI). The analyses were performed for the same geometrical and mechanical properties used in the former section (3.2.1) while choosing the inter-bridge spacing of (S= 20 m) as shown in figures (37) and (38). The numerical analyses have been conducted under the seismic loading record of Turkey (Kocaeli,1999). The employed mesh revealed in figures (37) and (38) includes (8104) zones of (8) nodes and (690) three-dimensional structural elements of 2 nodes. Unpredictably the plasticity under the isolated light perpendicular bridge of (M_{st}= 350 T) has prolonged heavily and deeply to the base of the soil, whereas the plasticity spread is substantially smaller under the central portion of the cap of the heavy perpendicular bridge of (M_{st}= 1050 T) as illustrated in figure (39). The interaction between the three bridges has incited a substantial change in the plasticity extension through the soil. The interaction between the three bridges in figure (40a) has reduced considerably the plasticity under the heavy bridge of (M_{st}= 1050 T) with a slight effect on the zones under the light bridge of (M_{st}= 350 T) and inter-bridges zones. Moreover, figure (40b) demonstrates that the plasticity extension almost vanished under the three bridges in the case of interaction between three perpendicular bridges, but it has increased considerably under the heavy bridge for the crossing configuration as shown in figure (40c). Table 10 elucidates the valuable impact of the (SSSI) on both superstructure acceleration and the internal forces induced in the piles. Due to the interaction between the three bridges, the mass and cap accelerations of the heavy bridge have hugely reduced by (86.3 %) and (90.63 %) respectively. Similarly, the mass and cap accelerations of the light bridge have considerably dropped by (97.46 %) and (45.2 %) respectively. Moreover, the (SSSI) effects have incited a substantial decline in the bending moment and shear force in the piles of the heavy bridge by (up to 52.55 %) and (up to 78.6 %) respectively. Alike, for the piles of the light bridge, the bending moment, and the shear force have hugely decreased due to the (SSSI) effects by (up to 91.18 %) and (up to 91.27 %) respectively.

The minimum internal forces (bending moment and shear force) induced in the corner pile (7) of the heavy bridge of (M_{st}= 1050 T) have been obtained for the parallel bridge configurations with bending moment of (M_{min}= 1496 KN.m) and shear force of (T_{min}= 426.3 KN) as elucidated in table 10 and figure (41). Whereas the maximum bending moment (M_{max}= 2412 KN.m) and maximum shear force (T_{max}= 1274 KN) have been achieved in the case of crossing bridge configuration. Alongside, the minimum accelerations of the superstructure (mass and cap) accompanied by minimum shear force in the central pile (15) of the heavy bridge (M_{st}= 1050 T) occurred in the case of perpendicular bridges configuration as shown in table 10 and figure (42). It should be mentioned that the bending moment and the shear force of the heavy bridge vary by (37.9 %) and (66.5 %) respectively with the bridge configuration changing between (parallel, perpendicular, and crossing), while the configuration change of the bridges has a bigger influence on the superstructure acceleration by variation of up to 74.45 % as demonstrated in table 10.

Table 10 Influence of different positioning of three dissimilar bridges on the seismic response system

Position	a_{st} (m/s²)	a_{Cap} (m/s²)	Internal forces							
			Central piles				Corner Piles			
			Pile (2) **(M_{st}=350 T)**		Pile (15) **(M_{st}=1050 T)**		Pile (1) **(M_{st}=350 T)**		Pile (7) **(M_{st}=1050 T)**	
			M_{max} (KN.m)	T_{max} (KN)	M_{max} (KN.m)	T_{max} (KN)	M_{max} (KN.m)	T_{max} (KN)	M_{max} (KN.m)	T_{max} (KN)
One Perpendicular Bridge (M_{st}=350 T)	**20.1**	**11.5**	**3979**	**1268**			**4093**	**1330**		
One Perpendicular Bridge (M_{st}=1050 T)	**20.53**	**12.49**			**2196**	**1325**			**2061**	**1294**

Position	Bridge **(M_{st}=350 T)**		Bridge **(M_{st}=1050 T)**		Three dissimilar bridges							
					Pile (2)		Pile (15)		Pile (1)		Pile (7)	
	a_{st}	**a_{Cap}**	**a_{st}**	**a_{Cap}**	**(M_{st}=350 T)**		**(M_{st}=1050 T)**		**(M_{st}=350 T)**		**(M_{st}=1050 T)**	
Parallel	**11.6**	**11.6**	**5.78**	**4.58**	**2091**	**1189**	**1260**	**294.8**	**1929**	**1236**	**1496**	**426.3**
Perpendicular	**0.54**	**6.47**	**2.81**	**1.17**	**411.8**	**113.4**	**1580**	**282.7**	**388**	**130.5**	**1578**	**456.2**
Crossing	**0.51**	**6.3**	**5.67**	**2.39**	**370.2**	**110.6**	**1042**	**589.7**	**360.8**	**123.2**	**2412**	**1274**

Contrarily, the minimum internal forces (bending moment and shear force) induced in the central and corner piles of the light bridge of (M_{st}= 350 T) have been achieved for the configuration of crossing bridges as illustrated in table 10 and figures (43) and (44). Precisely, the minimum bending moment (M_{min}=360.8 KN.m) has been obtained in the corner pile (1), while the minimum shear force (T_{min}= 110.6 KN) was attained in the central pile (2). Moreover, the minimum superstructure accelerations have been gained also for the crossing configuration with mass and cap accelerations of (A_{st}= 0.51 m/se^2) and (A_{cap}= 6.3 m/sec^2). It is worth noting that the mass accelerations of the light bridges for the perpendicular and crossing configurations are hugely smaller than the cap accelerations. Table 10 indicates an evident tendency to a significant drop in the superstructure acceleration, bending moment, and shear force by up to (95.6 %), (82.3 %), and (90.69 %) with the bridge configuration change starting from parallel to perpendicular and finally crossing bridges.

Table 10 and figure (45a) reveal a significant drop in the acceleration of the lumped mass of the heavy bridge of (M_{st}= 1050 T) with (A_{st}= 2.81 m/sec^2) in the case of perpendicular bridges configuration, while the mass accelerations values for the parallel and crossing bridges configurations are very close. In addition, it is worth noting the time lag between the three accelerations. Contrarily, the maximum lumped mass acceleration of the light bridge of (M_{st}=350 T) has been obtained for

the configuration of the parallel bridges with (A_{st}= 11.6 m/sec^2), whereas the mass accelerations for the perpendicular and crossing configurations are hugely smaller and has semi-constant value as shown in figure (45b). Figure (46a) shows the Fourier spectral analyses of the lumped mass velocity of (M_{st}= 1050 T) for the three studied configurations. The dominant frequency of the parallel configuration (F= 0.827 Hz) dropped to (F= 0.6 Hz) for the crossing configuration and to (F= 0.473 Hz) for the perpendicular configuration. Conversely, for the dominant frequency of the lumped mass of (M_{st}=350 T) shown in figure (46b), the dominant frequencies are constant (F=0.7 Hz) for the three configurations, but with much smaller amplitude for the perpendicular and crossing configurations.

4. Conclusions

An extensive set of detailed 3D numerical analyses have been performed to evaluate the effects of Structure-Soil-Structure-Interaction (SSSI) between three dissimilar neighboring bridges under seismic excitations. The analyses have focused on the impact of the adjacent superstructures lumped masses ratios (200 %, and 300%) on the (SSSI) effect. Moreover, the effects of the prominent factors such as the inter-bridge spacing, and the position of the three neighboring bridges towards each other and towards the seismic loading direction have been investigated. The three-dimensional code (FLAC 3D) based on the finite-difference elements method has been used in the numerical calculations, in which hysteretic damping has been considered for both soil and bridges, and linear assumptions have been put forward for the bridges and non-linear assumptions for the soil behavior to simulate the realistic seismic behaviour of the soil in this rigorous three-dimensional modeling. These numerical analyses have been performed under a real single record, the real record of Turkey (Kocaeli 1999). Further analysis under different earthquake records will be pursued in the future to confirm the conclusions drawn.

The main question of this research is in what situations the seismic Structure-Soil-Structure Interaction (SSSI) effect could be beneficial or detrimental for the individual elements of the system?

Furthermore, what are the key factors that may control the degree of multi-structural interactions?

This research has led to the following principal conclusions based on the cases studied:

- Intriguingly, the results revealed substantial beneficial effects of (SSSI) between the three dissimilar bridges on both superstructure acceleration and the internal forces induced in the piles, particularly for the case of neighbouring superstructures lumped masses ratio of (300 %). Differently, the (SSSI) effects between two identical bridges (M_{st}= 350 T) has modest effect (rather positive) on the seismic response of the two bridges and the internal forces induced in the piles, according to the results of Alfach and Al Helwani (2019).

- The consideration of (SSSI) effect between dissimilar bridges incites a sharp drop in the superstructure acceleration (up to 90.63 %) for the case of adjacent superstructures masses ratio of (300 %).

- The (SSSI) effect sharply reduce the bending moment and the shear force induced in the piles by (up to 91.18 %) and (up to 91.27 %) respectively for the case of neighbouring superstructures lumped masses ratio of (300 %).

- Substantially, in case of interaction between adjacent different bridges, the level of the (SSSI) effect on the response of the bridges highly depend on the neighboring superstructures lumped mass ratios.

-The inter-bridge spacings have slight effect on the superstructure acceleration by reduction of the closest spacing (up to 6.9 %). Similarly, the bending moment and the shear force decline by (up to 10.47 %) and (up to 14.38 %) respectively, which agrees with the conclusions obtained by Alfach and Al Helwani (2019) for the effect of inter-bridge spacing between two identical bridges of (M_{st}= 350 T).

- Finally, the geometrical position of the bridges towards each other and towards the seismic loading direction has significant impact on the seismic behavior of the system, particularly for the light bridges, which is reflected by huge

reduction for the crossing at 45^{o} case of the superstructure acceleration, the bending moment and the shear force by ratios up to (97.46 %), (91.18 %), and (91.27 %) respectively, which agrees with the results of Alfach and Al Helwani (2019) for the interaction between two identical bridges of (M_{st}= 350 T).

Declarations

Ethics Declaration

The authors declare that they have no conflict of interest.

References

Ada, M., and Ayvaz, Y., 2019. The structure-soil-structure interaction effects on the response of the neighbouring frame structures. *Latin American Journal of Solids and Structures*,16(8), e224. https://doi.org/10.1590/1679-78255762

Alam, Md Iftekharul., Kim, Dookie., 2014. Spatially varying Ground Motion Effects on Seismic Response of Adjacent Structures Considering Soil-Structure Interaction. *Advances in Structural Engineering,* Vol. 17 No. 1 2014. https://doi.org/10.1260/1369-4332.17.1.131

Álamo, Meneses., G. M., Padrón Hernández, L. A., Aznárez González, J. J., & Maeso Fortuny, O., 2015. Structure-soil-structure interaction effects on the dynamic response of piled structures under obliquely-incident seismic shear waves. *Soil dynamics and earthquake engineering,*Vol.78, 142-153. https://doi.org/10.1016/j.soildyn.2015.07.013

Alfach, Mohanad Talal., Al Helwani, Amjad., 2019. Seismic interactions between adjacent and crossing bridges on deep foundations in nonlinear soil. *Geomechanics and Geoengineering*. https://doi.org/10.1080/17486025.2019.1648883

Alfach, Mohanad Talal., 2020. Seismic structure-soil-structure interaction between two different adjacent piled bridges founded in nonlinear soil. *Geomechanics and Geoengineering*.

Andersen, L.V., Peplow, A., Bucinskas, P., Persson, P., Persson, K., 2017. Variation in models for simple dynamic structure–soil–structure interaction problems. *Procedia Engineering,*Vol. 199. https://doi.org/10.1016/j.proeng.2017.09.190

Bard, P. Y., Boutin, C., Dietz, M. S., Schwan, L., 2013. Study of multi-building interactions and site-city effects through an idealized experimental model, *Seismic Engineering Research Infrastructures for European Synergies,* Project No.: 227887, Final report.http://www.series.upatras.gr/sites/default/files/file/SERIES_SCIES_final%20report.pdf

Barrios, G., Chouw, N., 2015. Experimental investigations of interaction between structure, soil and adjacent structures, *In NZSEE Conference,* New Zealand.

Bolisetti, C., and Whittaker, A.S., 2015. Site Response, Soil-Structure Interaction and Structure-Soil-Structure Interaction for Performance Assessment of Buildings and Nuclear Structures, *Technical Report MCEER-15-0002, MCEER,* University at Buffalo. http://www.buffalo.edu/mceer/catalog.host.html/content/shared/www/mceer/publications/MCEER-15-0002.detail.html

Bolisetti, C., and Whittaker, A.S., 2020. Numerical investigations of structure-soil-structure interaction in buildings, *Engineering Structures,* 215 – 110709. https://doi.org/10.1016/j.engstruct.2020.110709

Bybordiani, M., and Arici, Y., 2019. Structure-soil-structure interaction of adjacent buildings subjected to seismic loading. *Earthq. Eng. Struct. Dyn*, 48, 731–748. https://doi.org/10.1002/eqe.3162

Gan, Jinsong., Li, Peizhen and Liu, Qiang., Chen, Jiang., 2017. Shaking table test of dynamic interaction of soil – high-rise buildings. *European Journal of Environmental and Civil Engineering*, *21:3, 249-271,* https://doi.org/10.1080/19648189.2015.1110057

Ge, Qi., Xiong, Feng., Zhang, Jing., 2020. Study on dynamic structure-soil-structure interaction of three adjacent tall buildings subjected to seismic loading. Sustainability, *12*(1), 336. https://doi.org/10.3390/su12010336

Ikeda, Y., Shimomura, Y., Nakamura, M., Haneda, O., Arai, T., 2004. Dynamic influence of adjacent structures on pile foundation based on forced vibration tests and earthquake observation. *13th World Conference on Earthquake Engineering,* Vancouver, B.C., Canada. https://www.iitk.ac.in/nicee/wcee/article/13_1869.pdf.

Isbiliroglu, Y., Taborda, R., Bielak, J., 2015. Coupled soil-structure interaction effects of building clusters during earthquakes. *Earthquake Spectra,*Vol.31, Issue1. https://doi.org/10.1193/102412EQS315M

Kim, Kyung Tae., 2014. Three-dimensional nonlinear seismic response of large-scale ground-structure systems. *University of California,* San Diego. Ph.D. dissertation, La Jolla, CA. https://escholarship.org/uc/item/3x7237xp

Knappett, J.A., Madden, P., Caucis, K., 2015. Seismic structure-soil-structure interaction between pairs of adjacent building structures. *Geotechnique*, 65, 429–441. https://doi.org/10.1680/geot.SIP.14.P.059

Larkin, T., Qin, X., Chouw, N., 2016. Effect of local site on sfsi of clustered structures. *Conference: NatHaz 16 - Soil characterization and site effects, S. Miguel, Portugal.*

Lu, Yang., Li, Bo., Xiong, Feng., Ge, Qi., Zhao, Peng., Liu, Yang., 2020. Simple discrete models for dynamic structure-soil-structure interaction analysis. *Engineering Structures*. Volume 206, 110188. https://doi.org/10.1016/j.engstruct.2020.110188

Mason, H. B., Trombetta, N. W., Gille, S., Lund, J., Zupan, J., Jones, K. C., Puangnak, H., Bolisetti, C., Bray, J., Hutchinson, T., Fiegel, G., Kutter, B. L., Whittaker, A. S., 2010a. Seismic Performance Assessment in Dense Urban Environments: Centrifuge Data Report for HBM02 (Test 1). *Davis Center for Geotechnical Modeling, University of California*. Davis, California.

Nakamura, S., Nakamura, N., Suzuki, T., Inoda, K., Kosaka, K., 2012. Study on the Influence of Irregular Ground and Adjacent Building on the Seismic Response of Nuclear Power Plant Building. *15 WCEE*, LISBOA 2012. https://www.iitk.ac.in/nicee/wcee/article/WCEE2012_1367.pdf

Ngo, Van-Linh., Kim, Jae-Min., Chang, Soo-Hyuk and Lee, Changho., 2019. Effect of height ratio and mass ratio on structure-soil-structure interaction of two structures using centrifugal experiment. *Appl. Sci*, *9*(3), 526. https://doi.org/10.3390/app9030526

Ogut, oguz can., 2017. Soil-Structure Interaction Effect of Embedded Foundation and Adjacent Buildings on Response Characteristics of Superstructures. *Nagoya University*, *Nagoya. Ph.D. dissertation, Japan*.

Rahgozar, M.A., 2015. Accounting for soil nonlinearity in three-dimensional seismic structure-soil-structure-interaction analyses of adjacent tall buildings structures. *International journal of civil engineering,* 13 (3 and 4B) ,213-225. DOI: 10.22068/IJCE.13.3.213

Ritter, Stefan., 2017. Experiments in tunnel-soil-structure interaction. *Thesis (PhD). Department of Engineering,* University of Cambridge.

Roy, Christine., Bolourchi, Said., & Eggers, Daniel., 2015. Significance of structure-soil-structure interaction for closely spaced structures. *Nuclear Engineering and Design,*Vol. 295, 680-687. https://doi.org/10.1016/j.nucengdes.2015.07.067

Schwan, L., Boutin, C., Padrón, L.A., Dietz, M.S., Bard, P.Y., Taylor, C., 2016. Site-city interaction: theoretical, numerical and experimental crossed-analysis. *Geophys. J. Int*,Vol. 205, Issue 2, 1006-1031. https://doi.org/10.1093/gji/ggw049

Trombetta, N.W., Mason, H.B., Hutchinson Tara, C., Zupan Joshua, D., Bray Jonathan, D., Kutter Bruce, L., 2014. Nonlinear soil-foundation-structure and structure-soil-structure interaction: centrifuge test observations. *Journal of Geotechnical and Geoenvironmental Engineering*, Vol. 140, Issue 5. https://doi.org/10.1061/(ASCE)GT.1943-5606.0001074

Wang, Huai-feng., 2018. Structure-soil-structure interaction between underground structure and surface structure, Earthquakes - Forecast, *Prognosis and Earthquake Resistant Construction*, Valentina Svalova, IntechOpen. DOI: 10.5772/intechopen.76243

Yahyai, M., Mirtaheri, M., Mahoutian, M., Daryan, A. S. & Assareh, M. A., 2008. Soil structure interaction between two adjacent buildings under earthquake load. *American Journal of Engineering and Applied Sciences*, 1(2), 121-125. https://doi.org/10.3844/ajeassp.2008.121.125

Figures

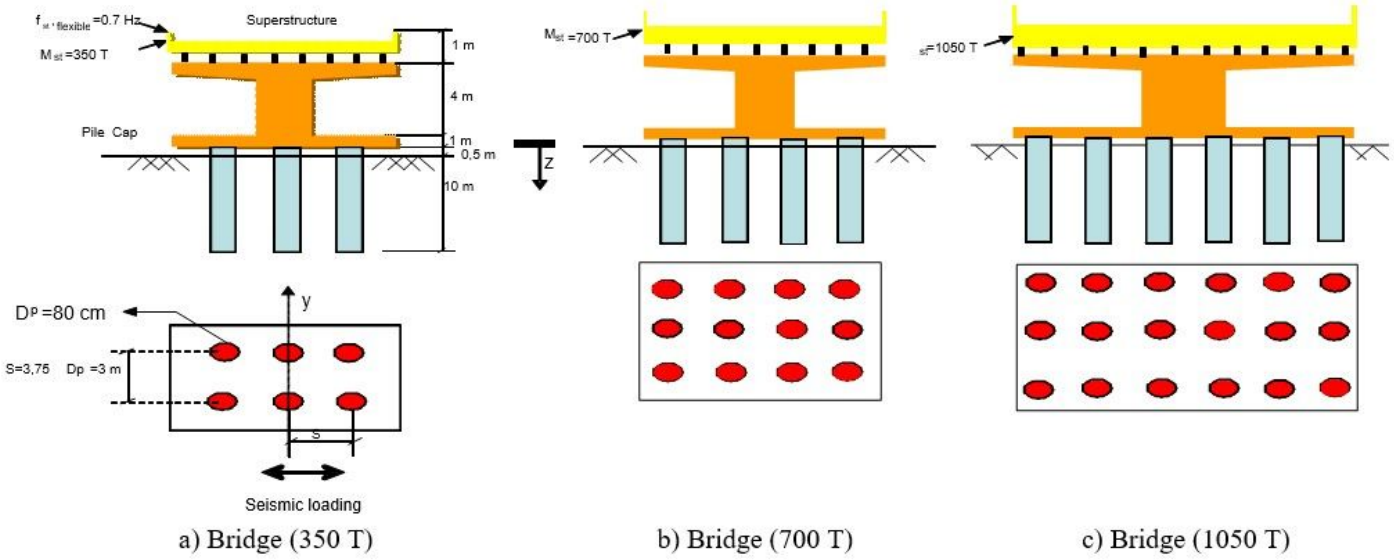

Figure 1

Piles-Bridge system geometry

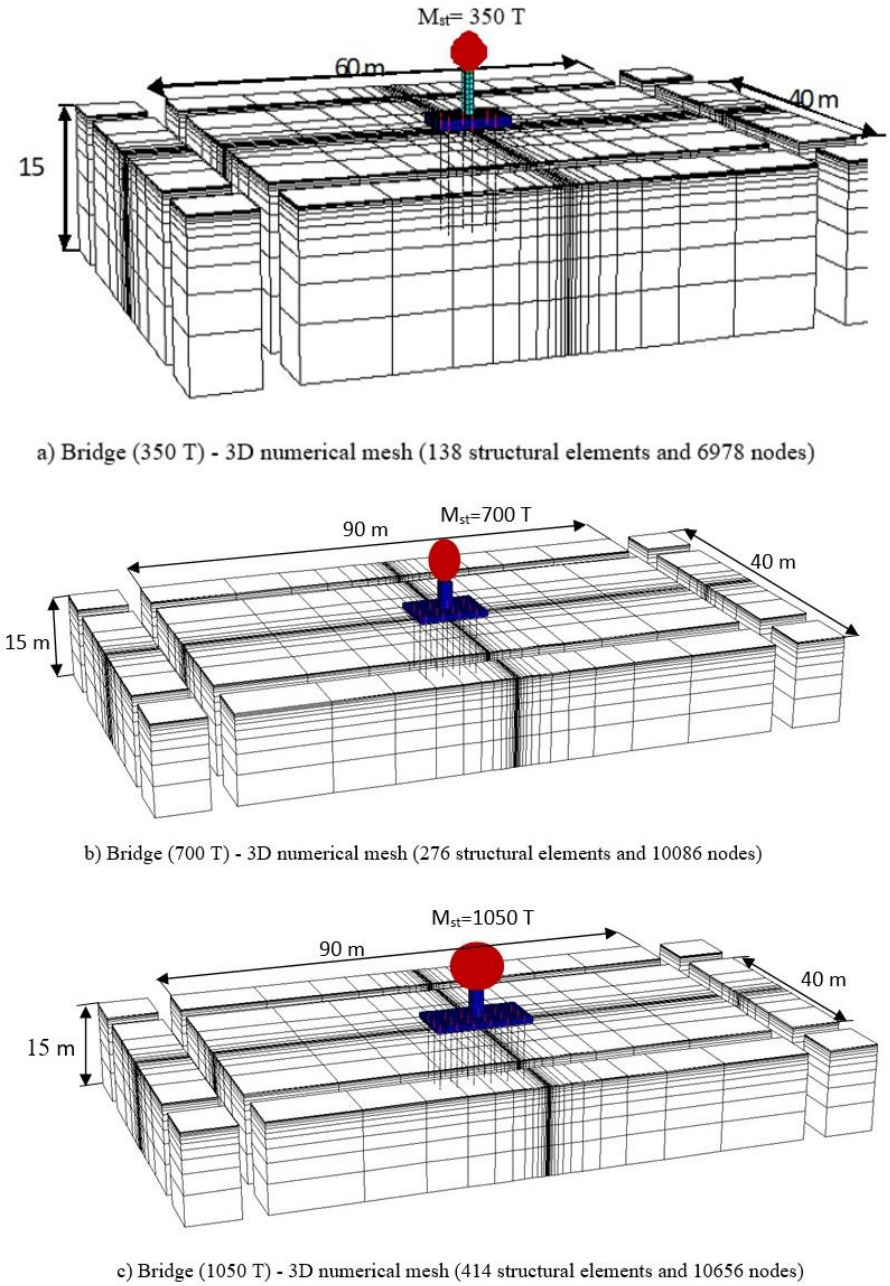

Figure 2

3D numerical mesh of Soil-Piles-Bridge System.

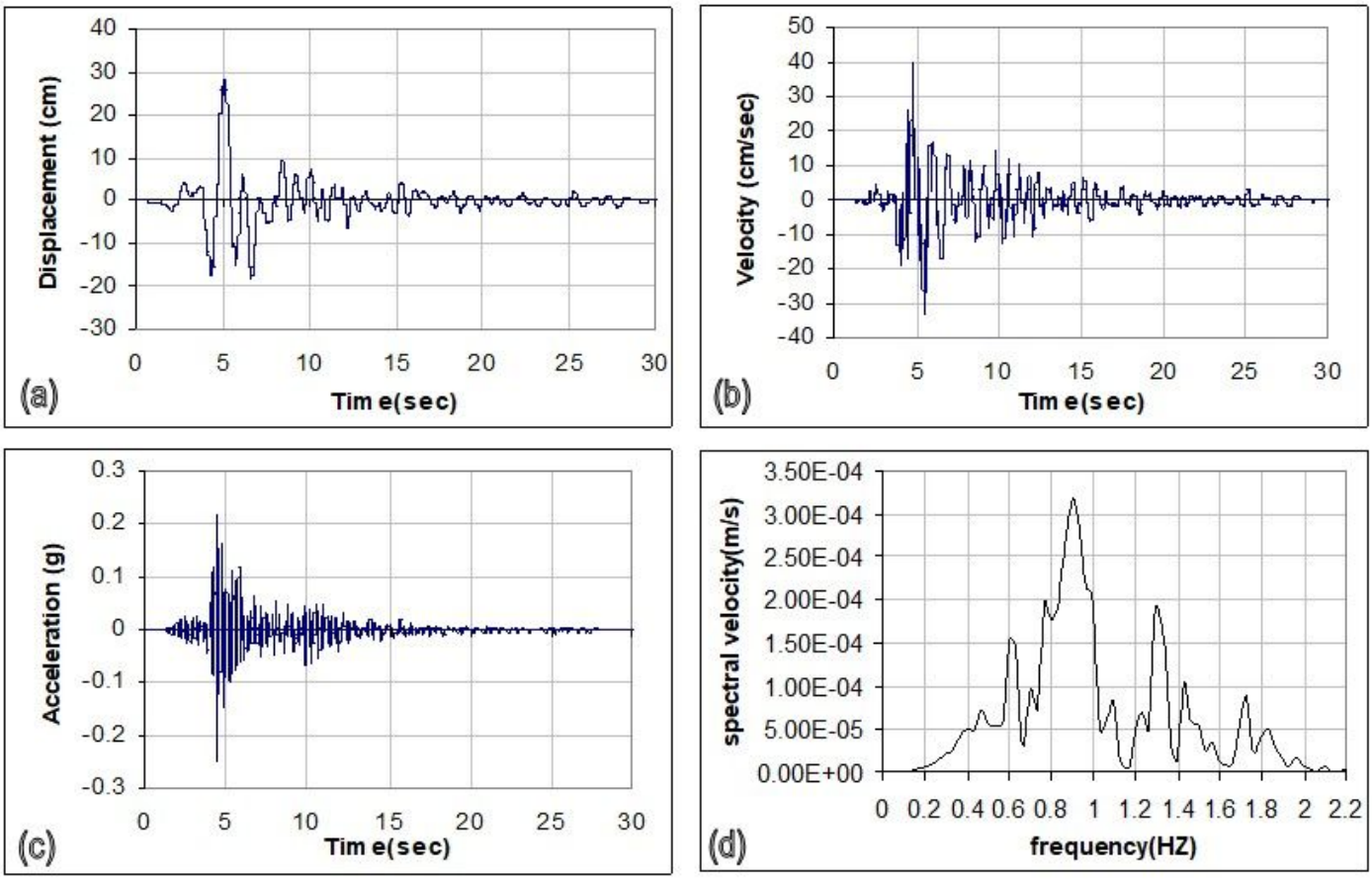

a) Displacement, b) Velocity, c) Acceleration, d) Fourier Spectra of Velocity Component.

Figure 3

Kocaeli earthquake record (1999)

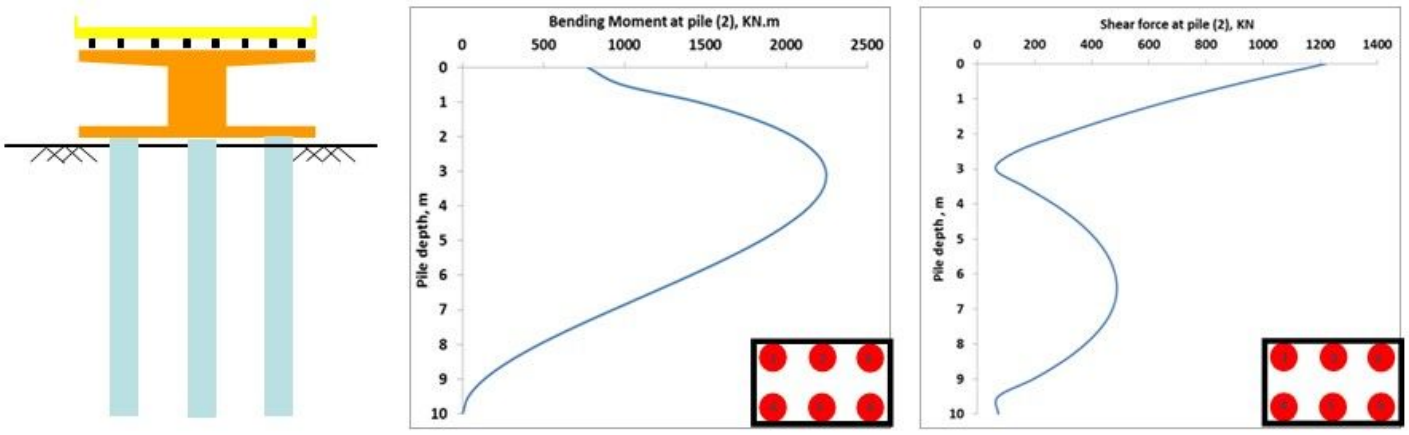

a) Maximum Bending Moment b) Maximum Shear Force

Figure 4

Internal forces at central pile (2).

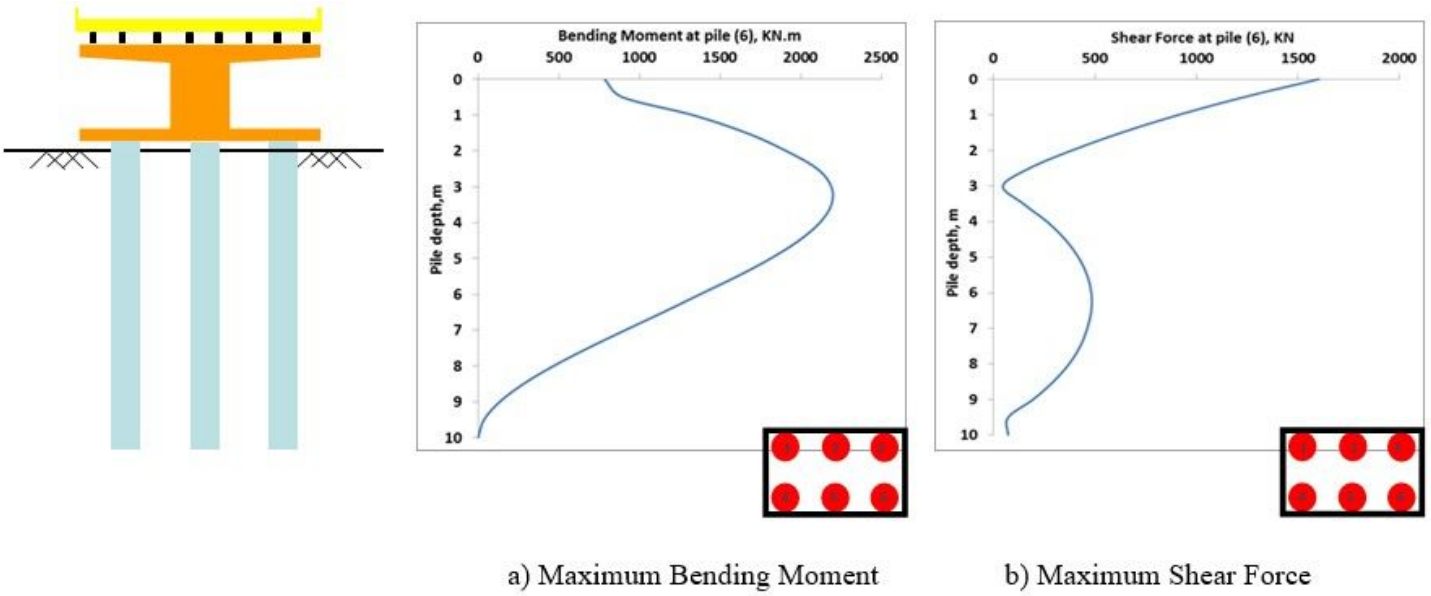

Figure 5

Internal forces at corner pile (6).

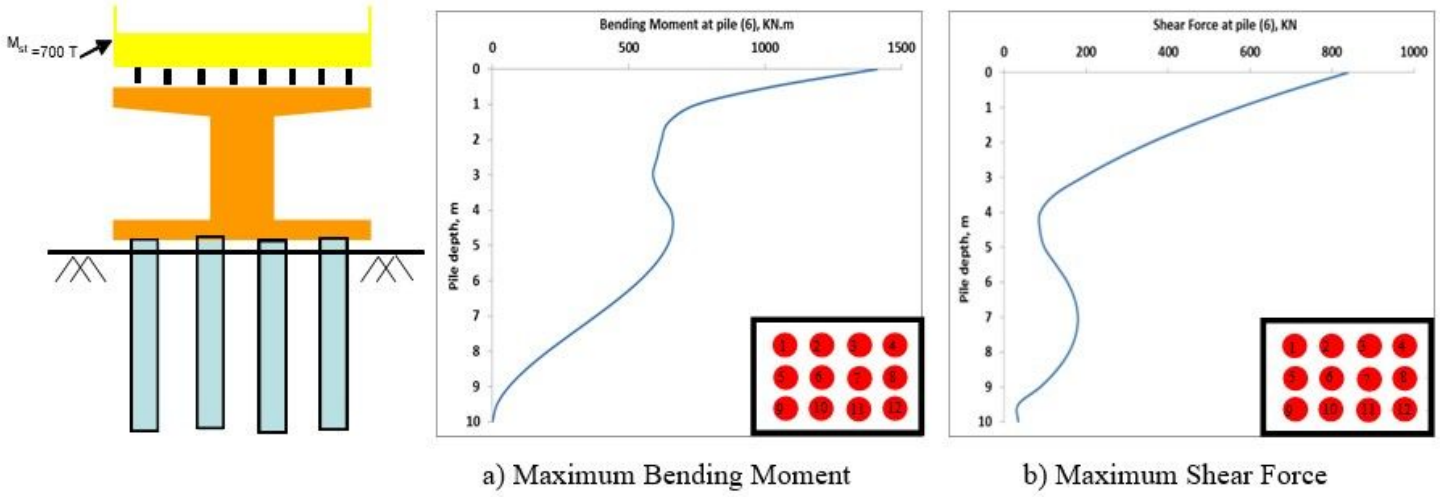

Figure 6

Internal forces at central pile (6).

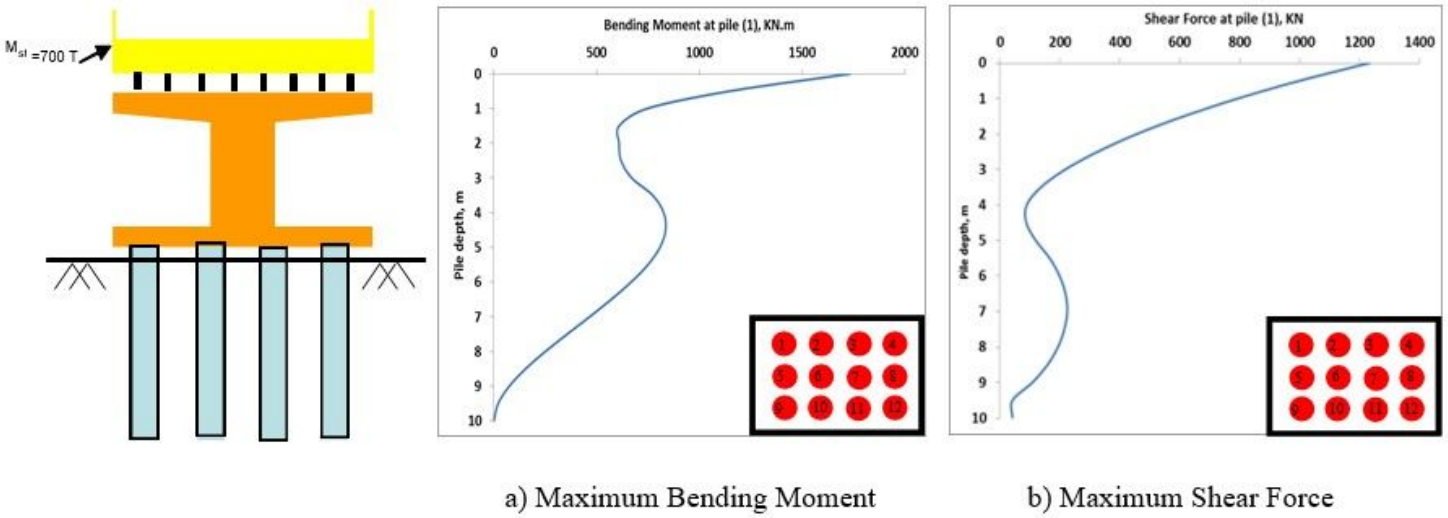

a) Maximum Bending Moment b) Maximum Shear Force

Figure 7

Internal forces at corner pile (1).

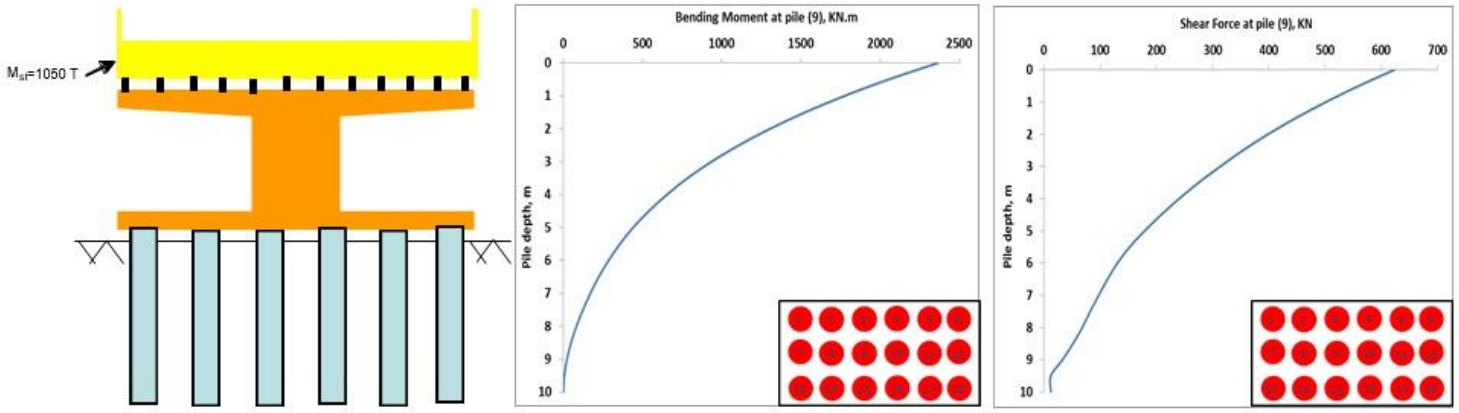

a) Maximum Bending Moment b) Maximum Shear Force

Figure 8

Internal forces at central pile (9).

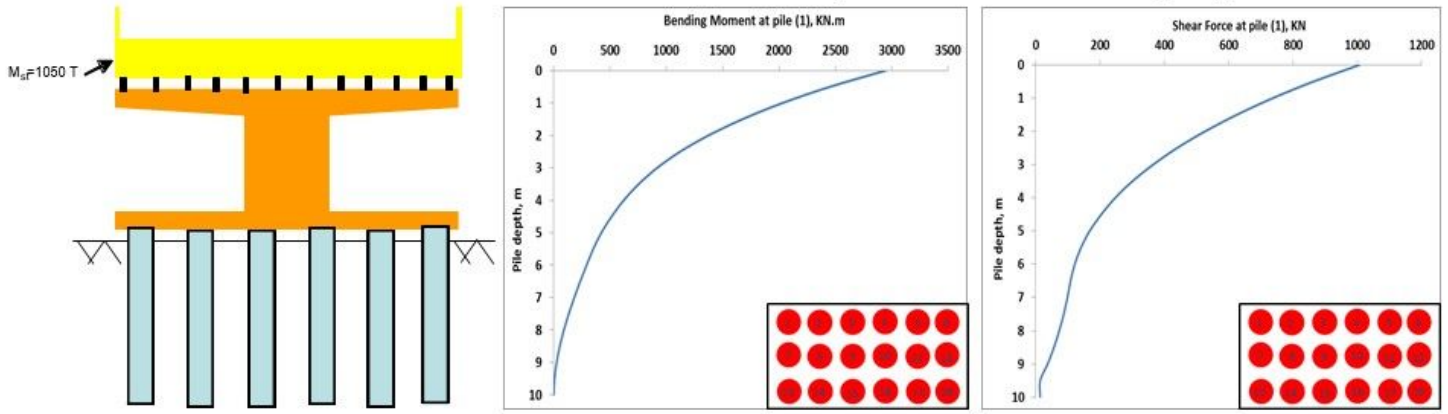

a) Maximum Bending Moment b) Maximum Shear Force

Figure 9

Internal forces at corner pile (1).

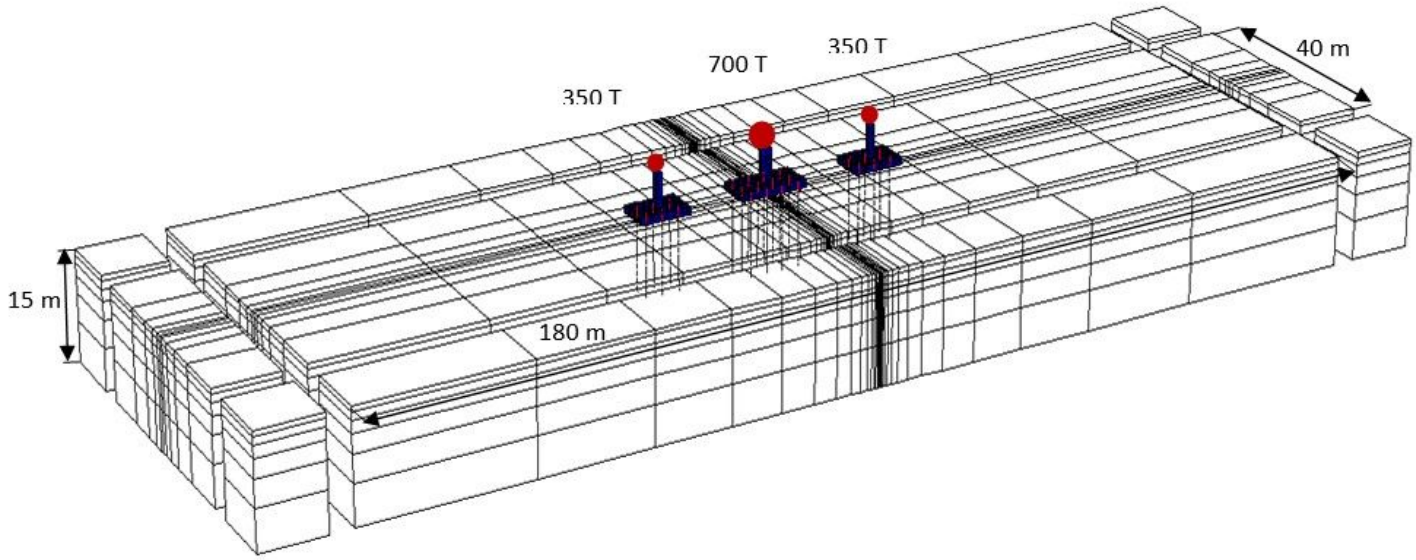

Figure 10

Parallel bridges System 3D numerical mesh with adsorbing boundaries (552 structural elements and 41361 nodes)

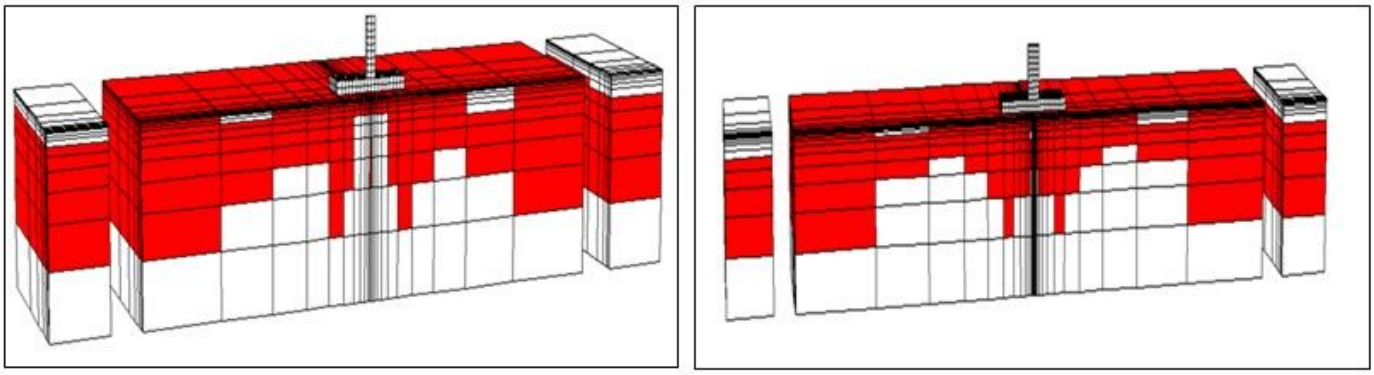

Figure 11

Distribution of plasticity (red zones) for two single isolated bridges (Mst=350 T) and (Mst=700 T).

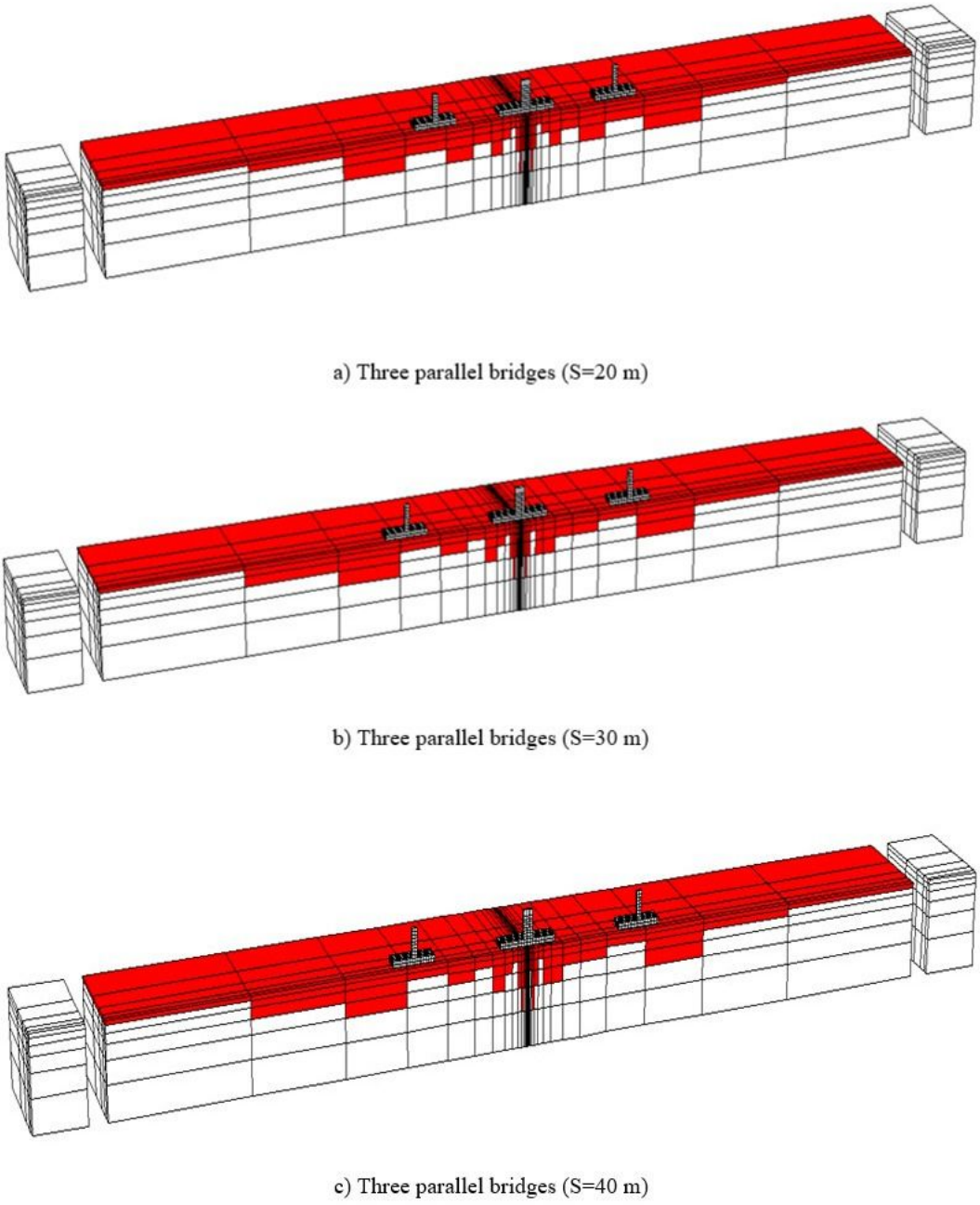

Figure 12

Distribution of plasticity (red zones) for different spacing between the three dissimilar bridges (Mst= 350 T, Mst= 700 T, Mst= 350 T)

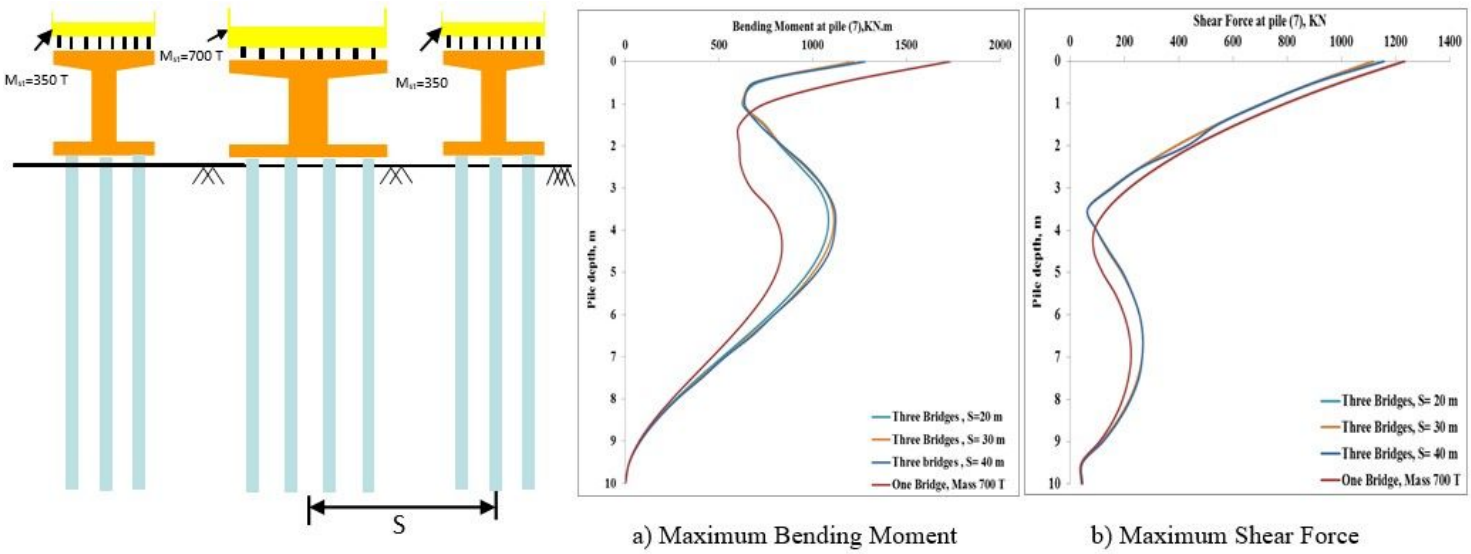

Figure 13

Three dissimilar parallel bridges: Internal forces at corner pile (7) of bridge (700 T)

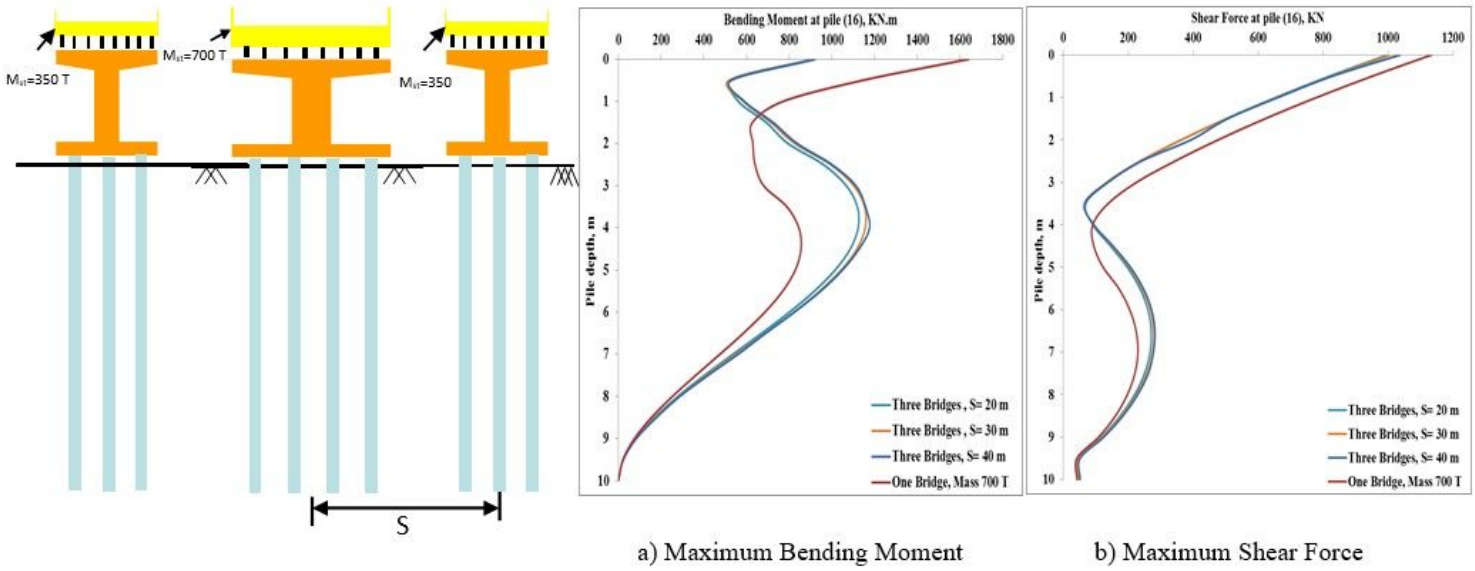

Figure 14

Three dissimilar Parallel bridges: Internal forces at central pile (16) of bridge (700 T)

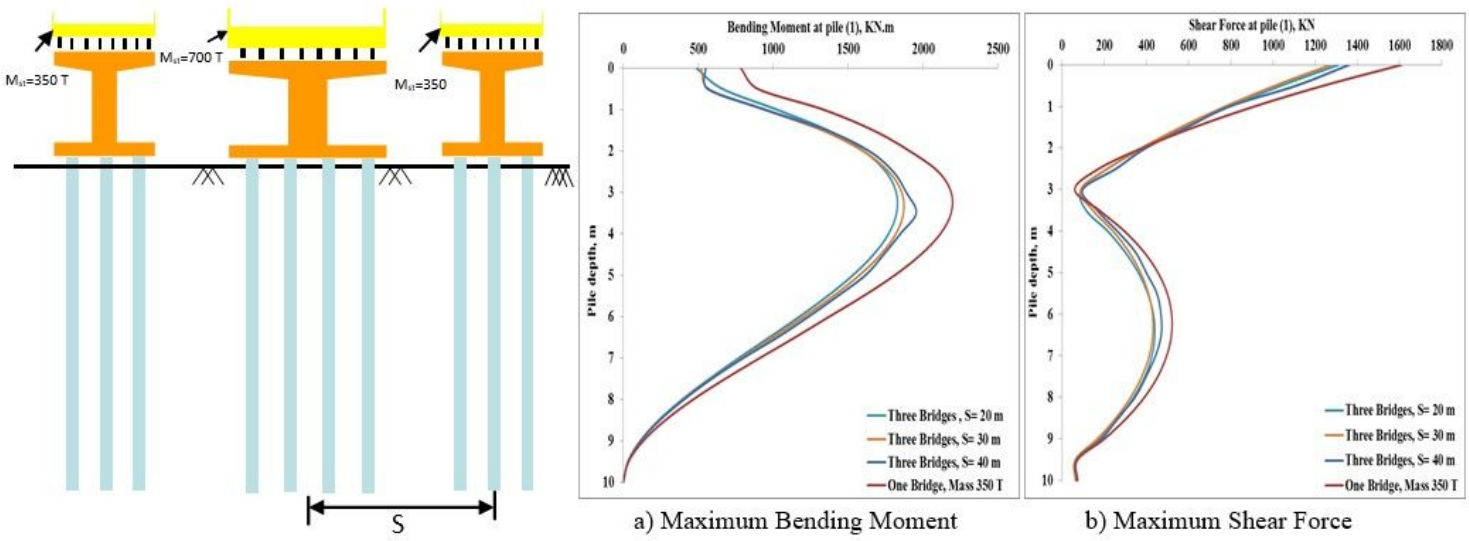

Figure 15

Three dissimilar parallel bridges: Internal forces at corner pile (1) of bridge (350 T)

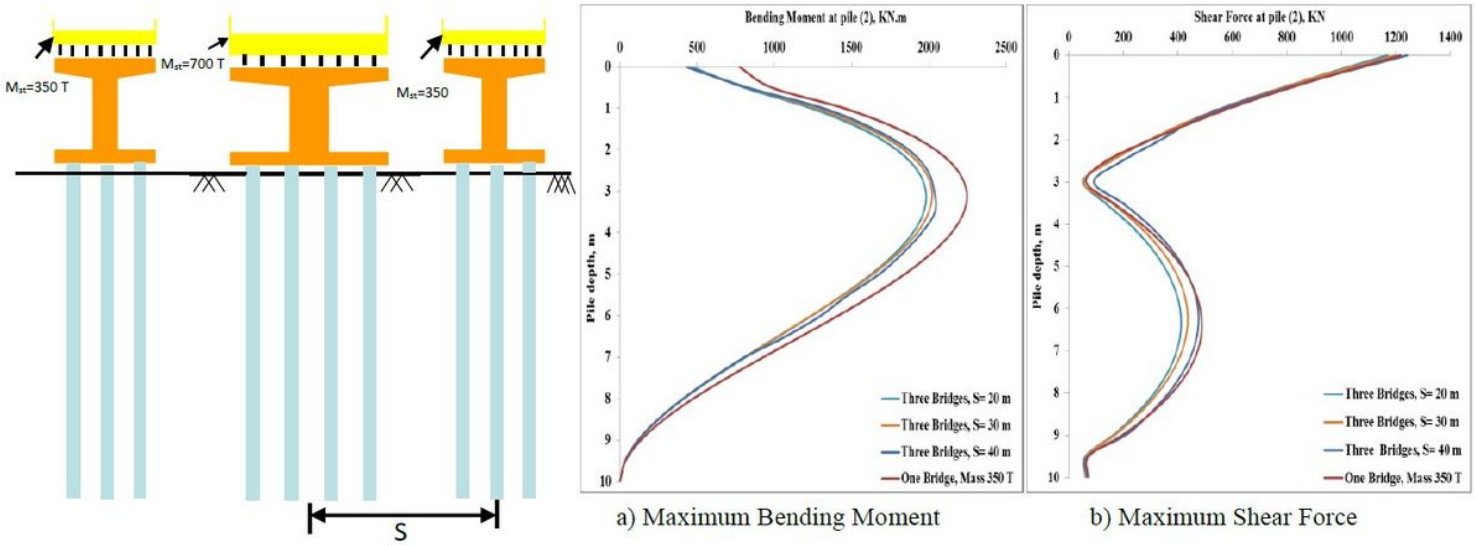

Figure 16

Three dissimilar parallel bridges: Internal forces at central pile (16) of bridge (350 T)

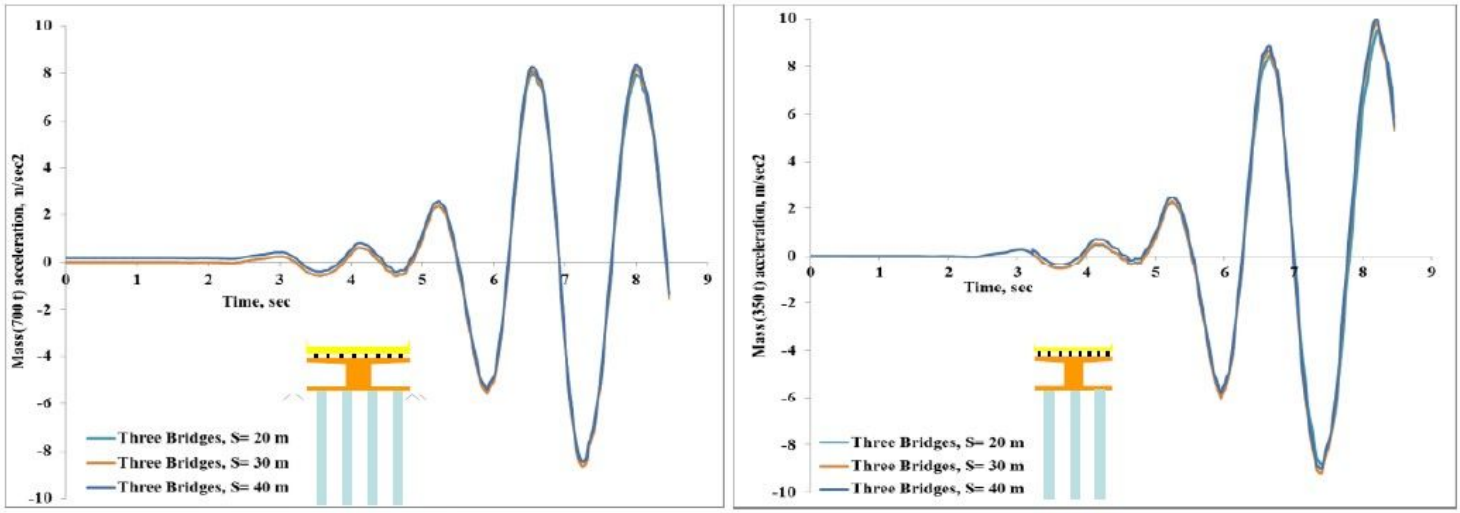

a) Mass (700 T) Acceleration b) Mass (350 T) Acceleration

Figure 17

Three dissimilar parallel bridges: Masses Accelerations.

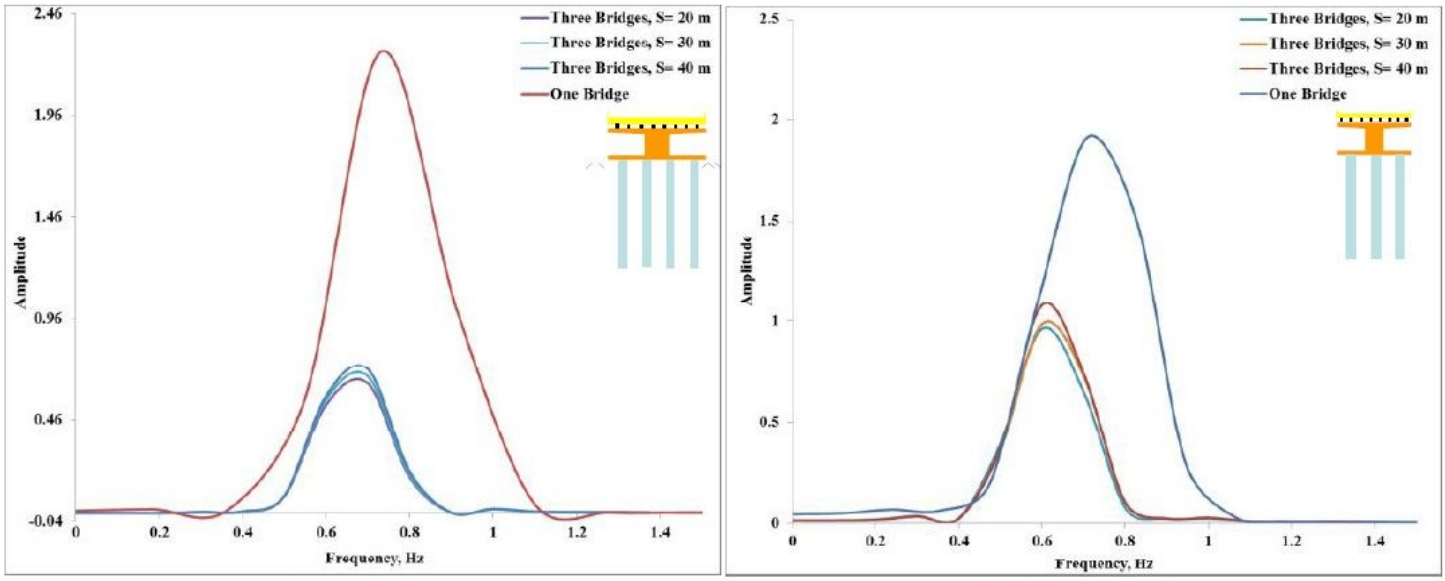

a) Mass (700 T) b) Mass (350 T)

Figure 18

Three dissimilar parallel bridges: Fourier spectra diagram.

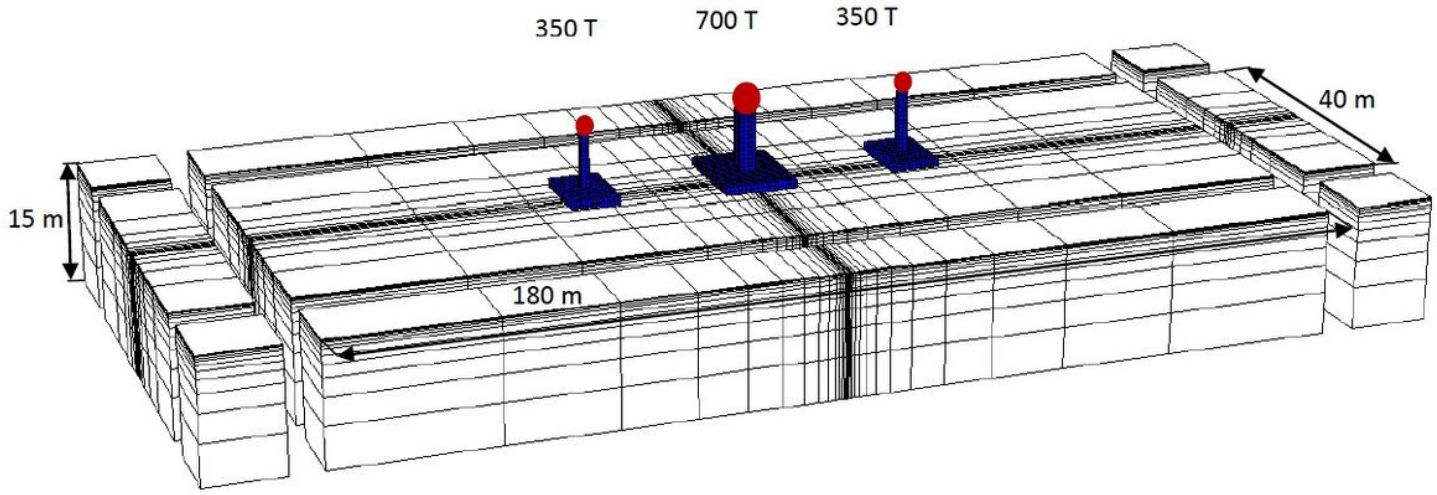

Figure 19

Perpendicular Bridges System 3D numerical mesh with adsorbing boundaries (552 structural elements and 77990 nodes)

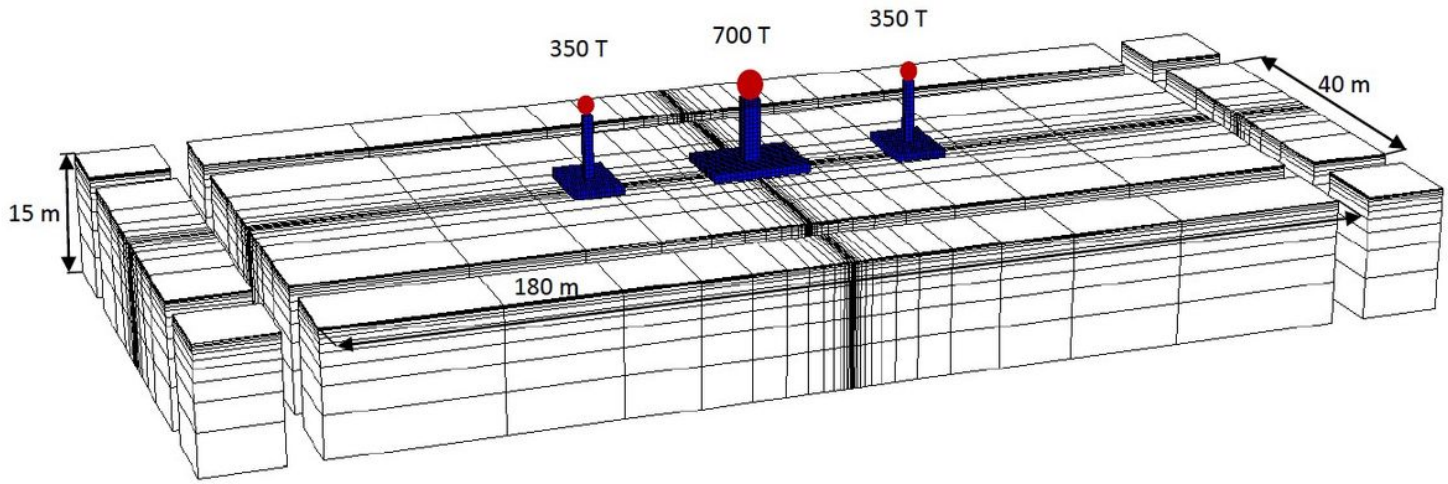

Figure 20

Crossing Bridges System 3D numerical mesh with adsorbing boundaries (552 structural elements and 77990 nodes)

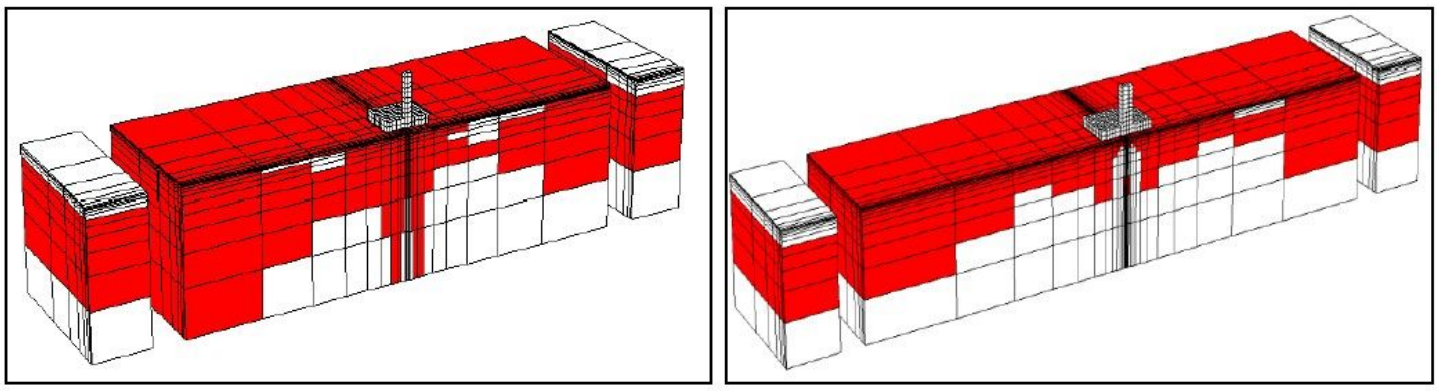

a) One perpendicular bridge (M_{st}=350 T)

b) One perpendicular bridge (M_{st}=700 T)

Figure 21

Distribution of plasticity for two single isolated bridges (Mst=350 T) and (Mst=700 T).

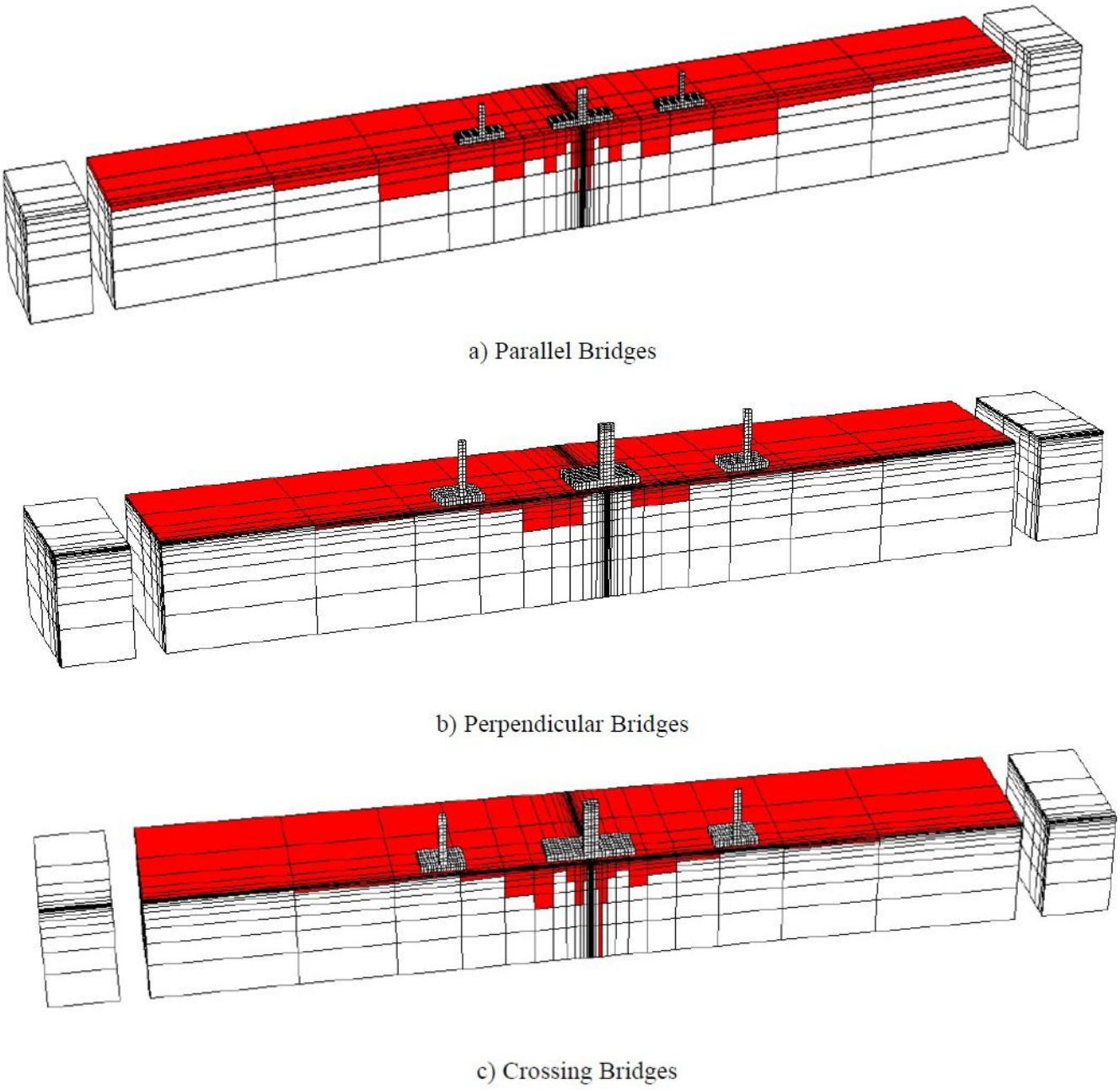

a) Parallel Bridges

b) Perpendicular Bridges

c) Crossing Bridges

Figure 22

Distribution of plasticity (red zones) for different positioning of the three dissimilar Bridges. (Mst= 350 T, Mst= 700 T, Mst= 350 T)

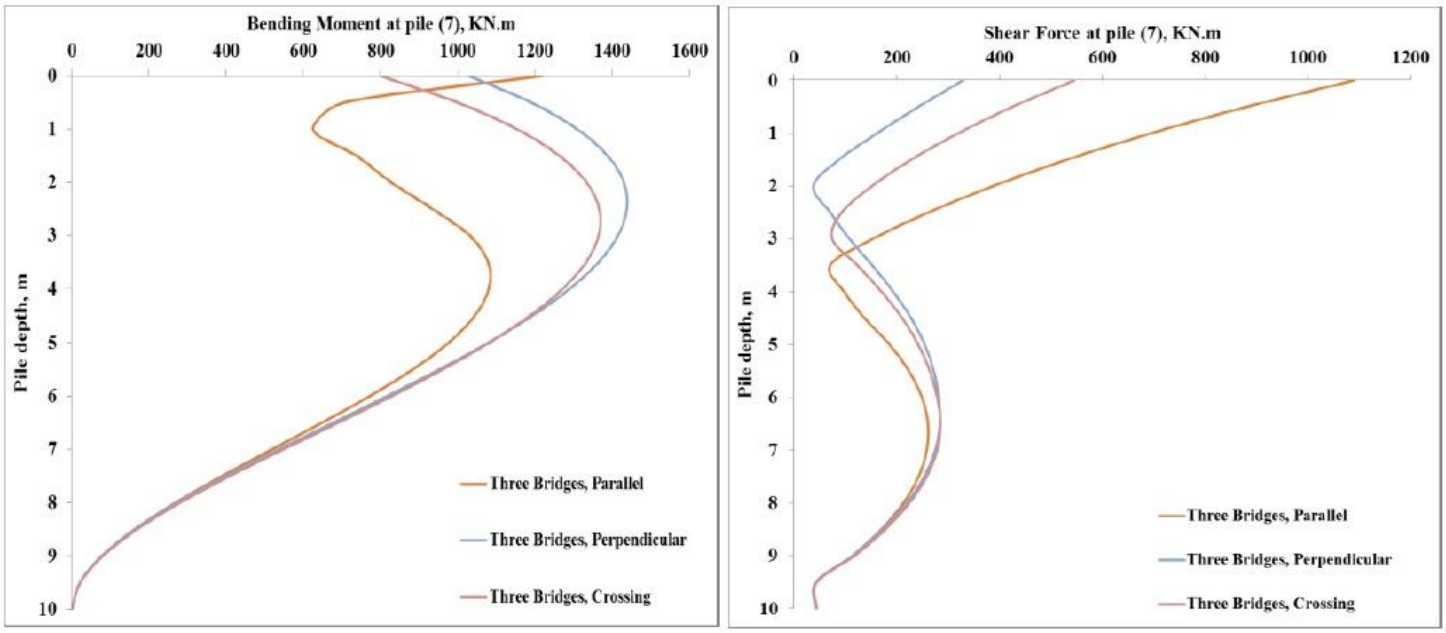

a) Maximum Bending Moment b) Maximum Shear Force

Figure 23

Three dissimilar bridges: Internal forces at corner pile (7) of bridge (700 T).

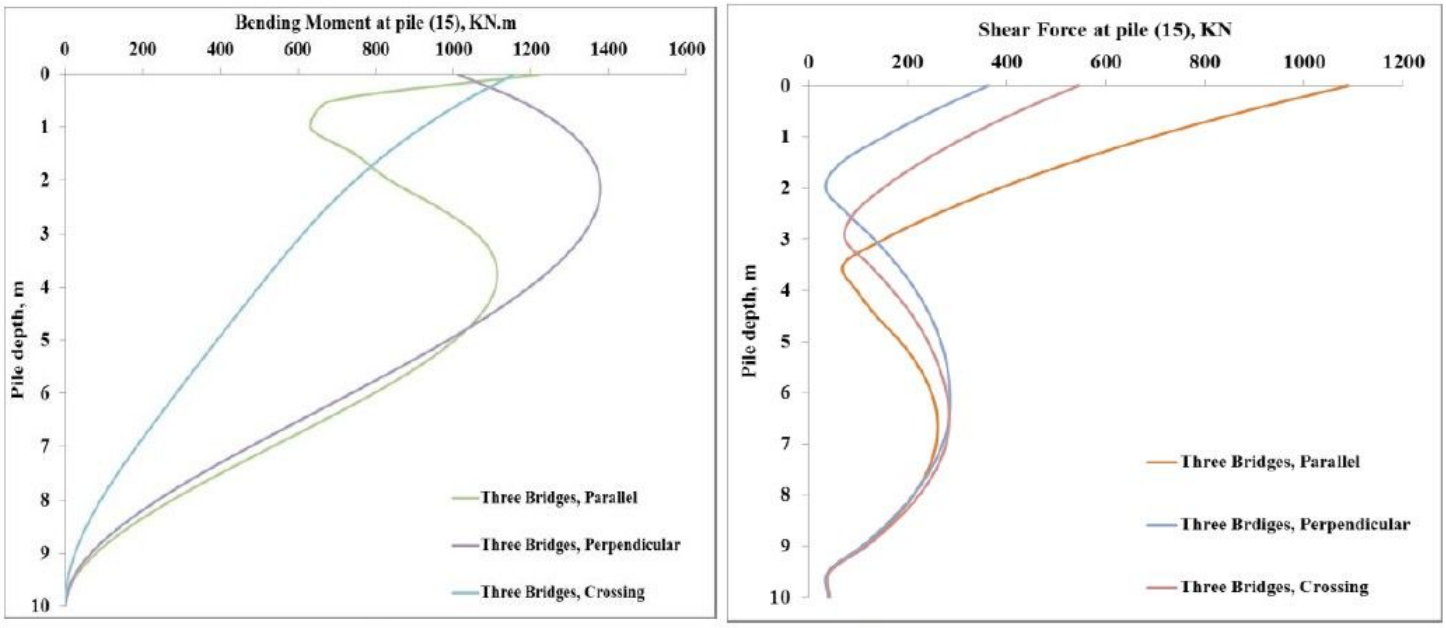

a) Maximum Bending Moment b) Maximum Shear Force

Figure 24

Three dissimilar bridges: Internal forces at central pile (15) of bridge (700 T).

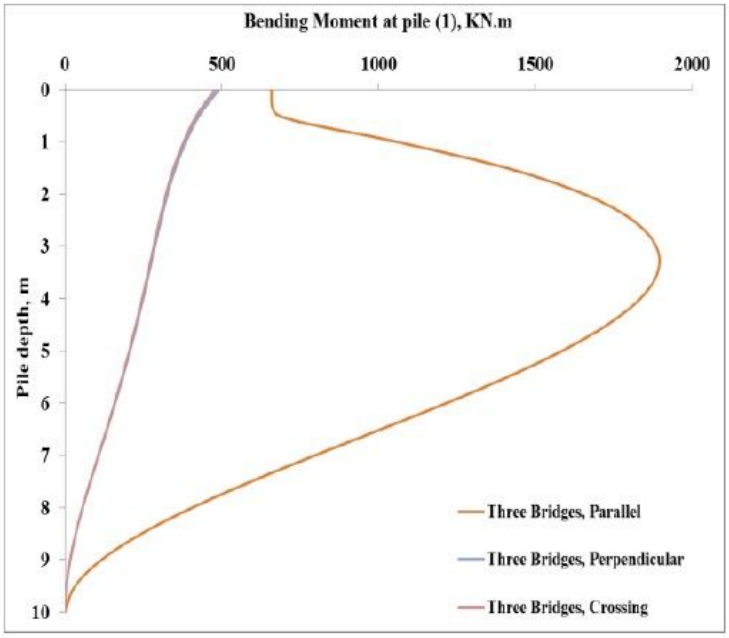

a) Maximum Bending Moment

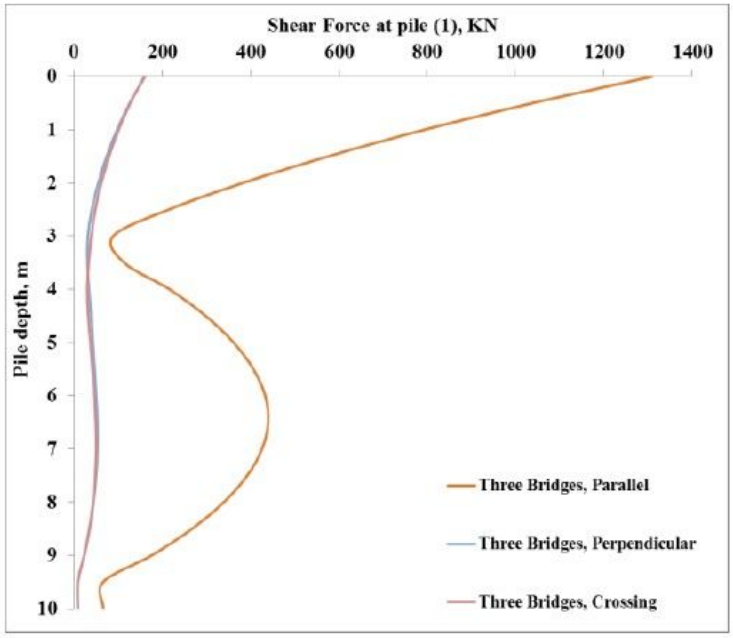

b) Maximum Shear Force

Figure 25

Three dissimilar bridges: Internal forces at corner pile (1) of bridge (350 T).

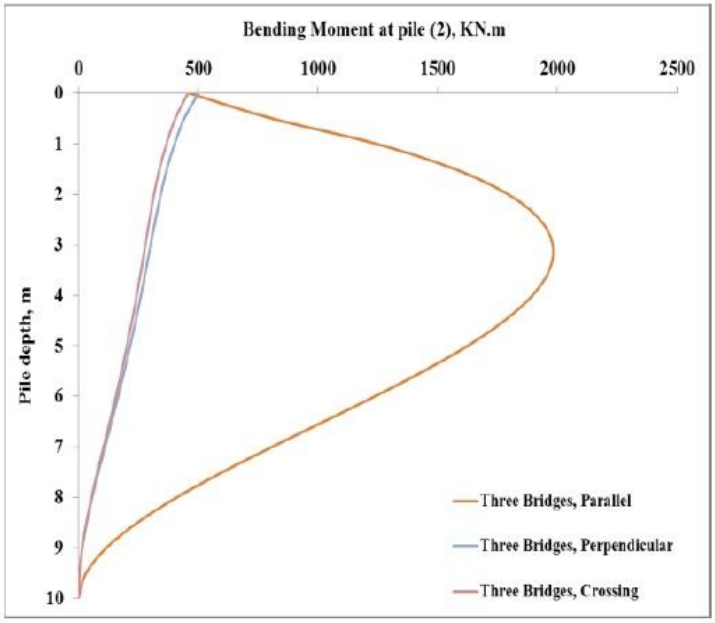

a) Maximum Bending Moment

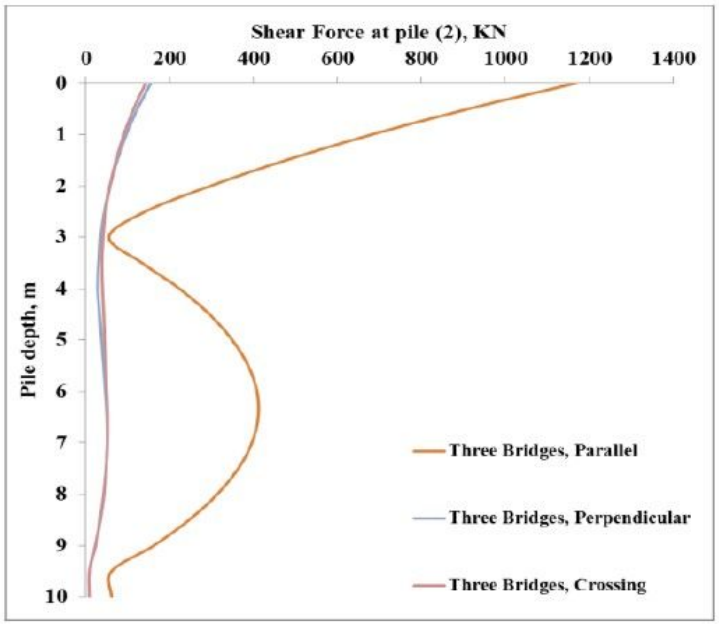

b) Maximum Shear Force

Figure 26

Three dissimilar bridges: Internal forces at central pile (2) of bridge (350 T)

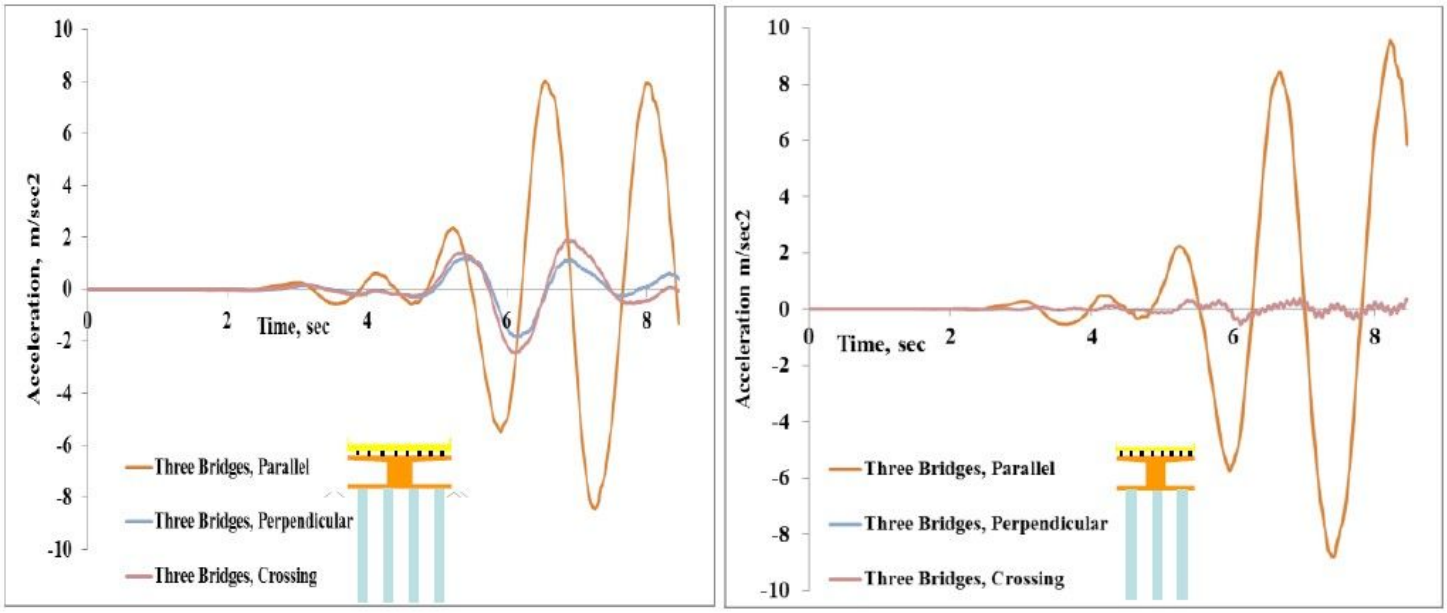

a) Mass (700 T) Acceleration

b) Mass (350 T) Acceleration

Figure 27

Three dissimilar bridges: Masses Accelerations.

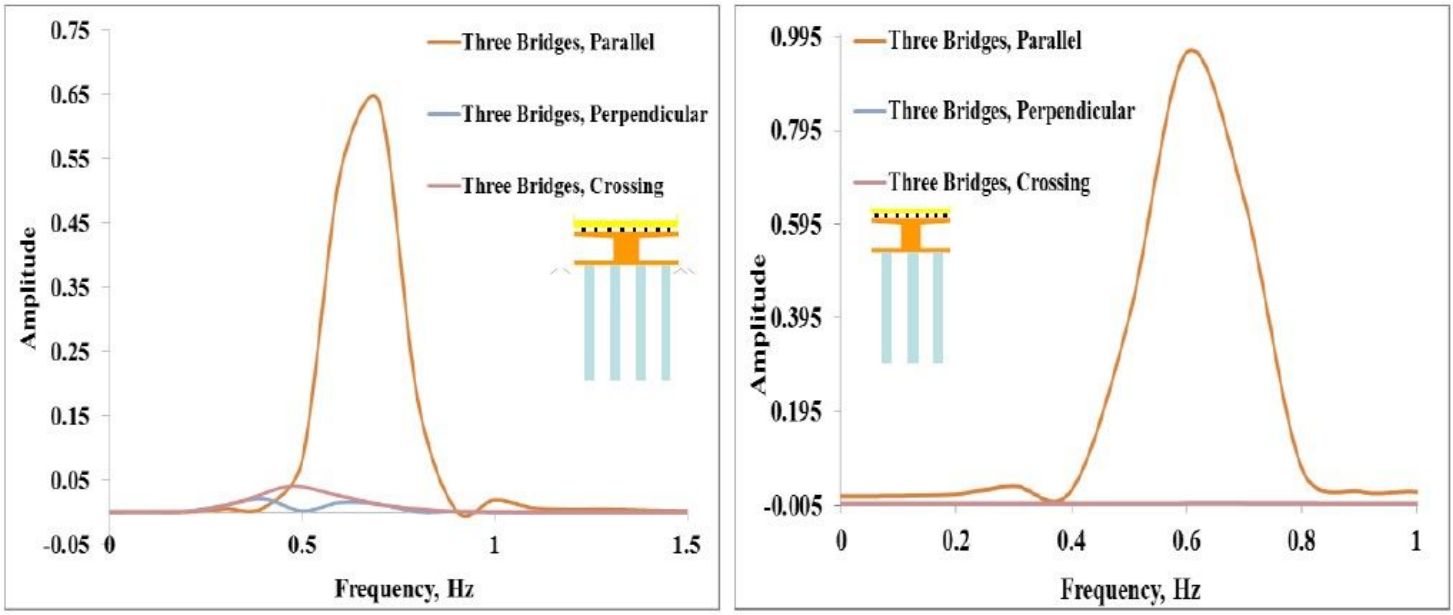

a) Mass (700 T)

b) Mass (350 T)

Figure 28

Three dissimilar bridges: Fourier spectra diagram.

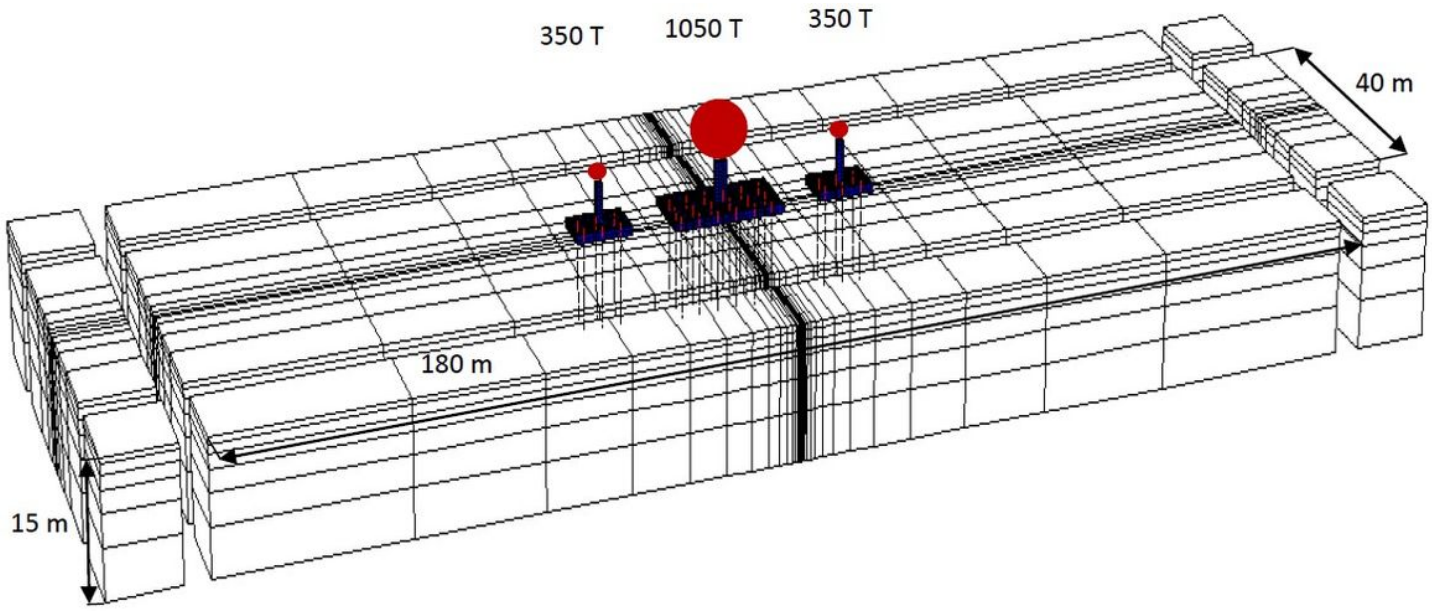

Figure 29

Parallel bridges System 3D numerical mesh with adsorbing boundaries (552 structural elements and 33072 nodes)

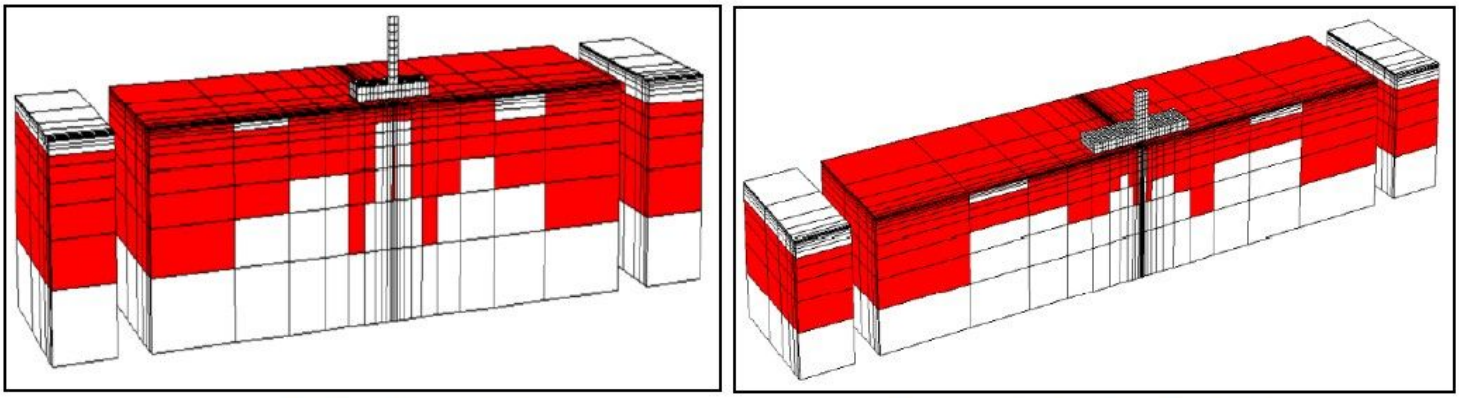

a) One bridge (M_{st}=350 T)

b) One bridge (M_{st}=1050 T)

Figure 30

Distribution of plasticity for two single isolated bridges (Mst=350 T) and (Mst=1050 T).

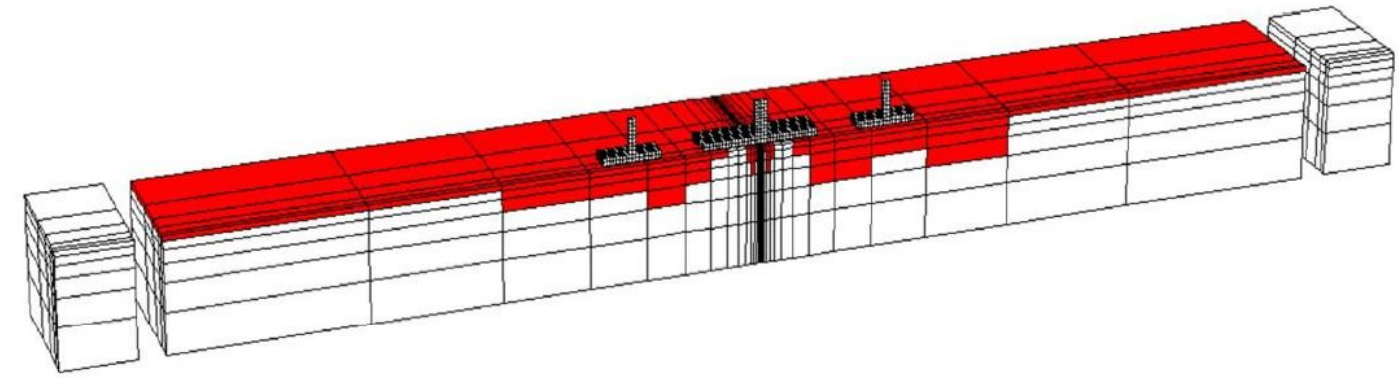

a) Three parallel bridges (S=20 m)

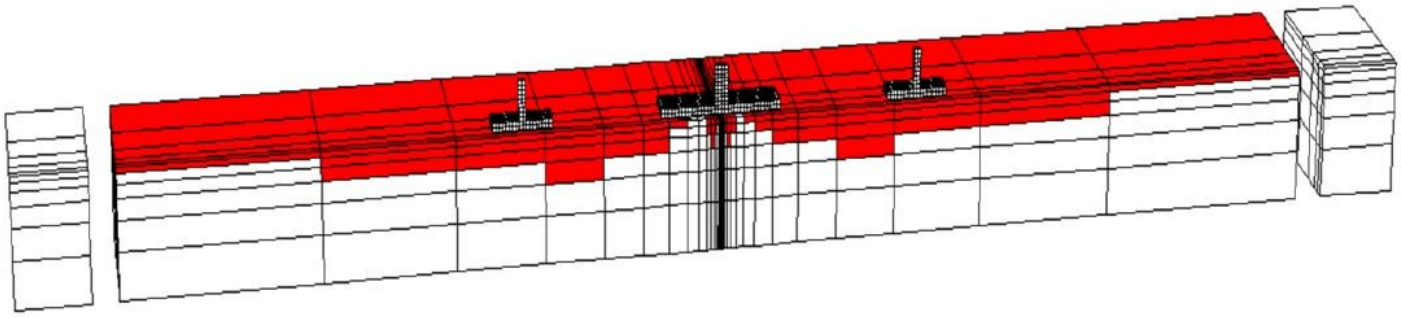

b) Three parallel bridges (S=30 m)

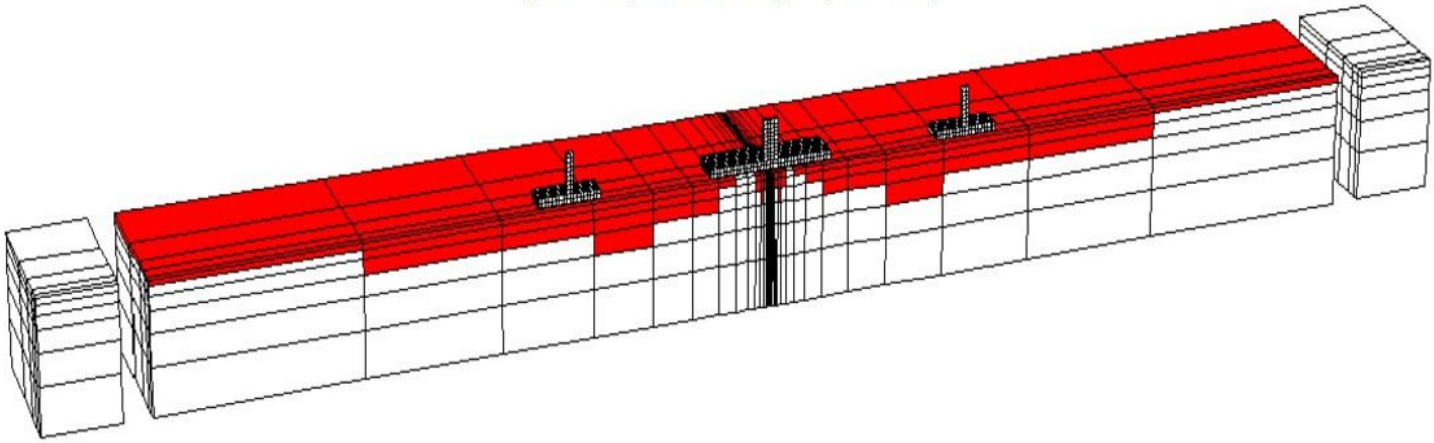

c) Three parallel bridges (S=40 m)

Figure 31

Distribution of plasticity (red zones) for different spacing between the three dissimilar bridges (Mst= 350 T, Mst= 1050 T, Mst= 350 T)

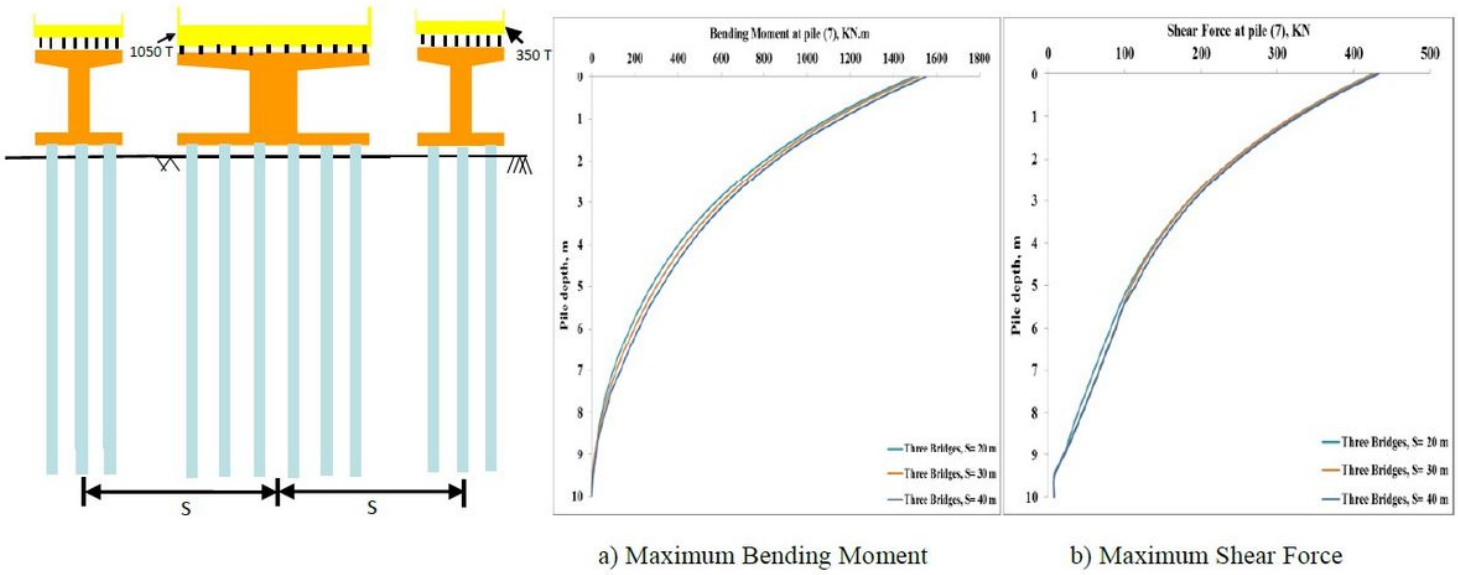

a) Maximum Bending Moment b) Maximum Shear Force

Figure 32

Three dissimilar parallel bridges: Internal forces at corner pile (7) of Bridge (1050 T).

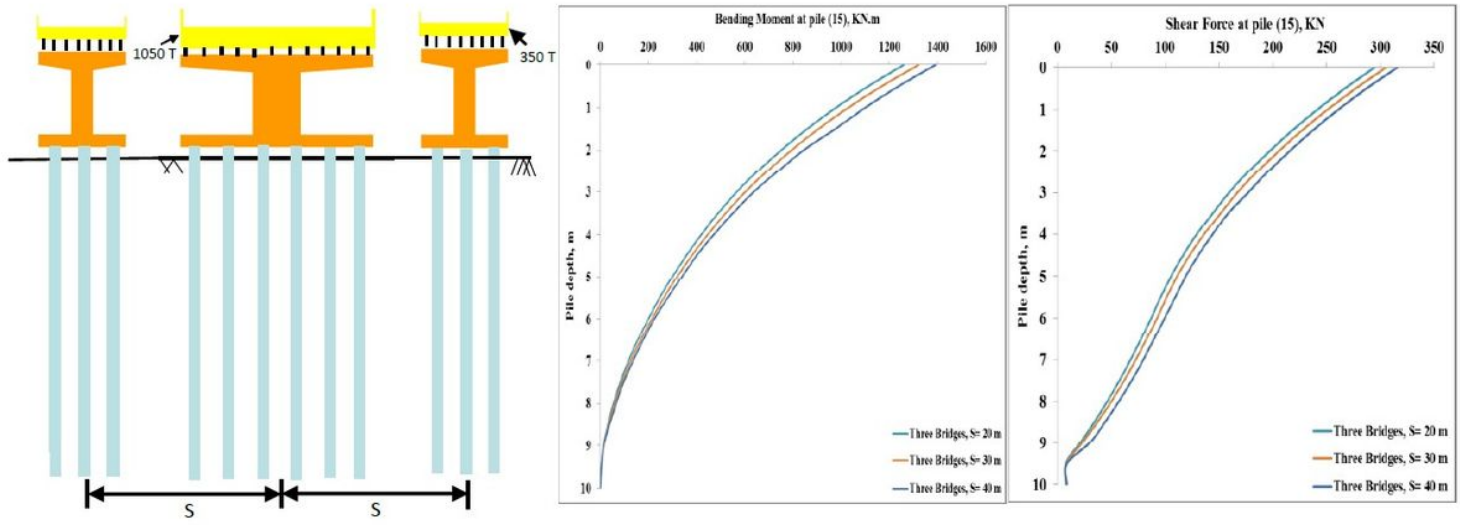

a) Maximum Bending Moment b) Maximum Shear Force

Figure 33

Three dissimilar parallel bridges: Internal forces at corner pile (15) of Bridge (1050 T).

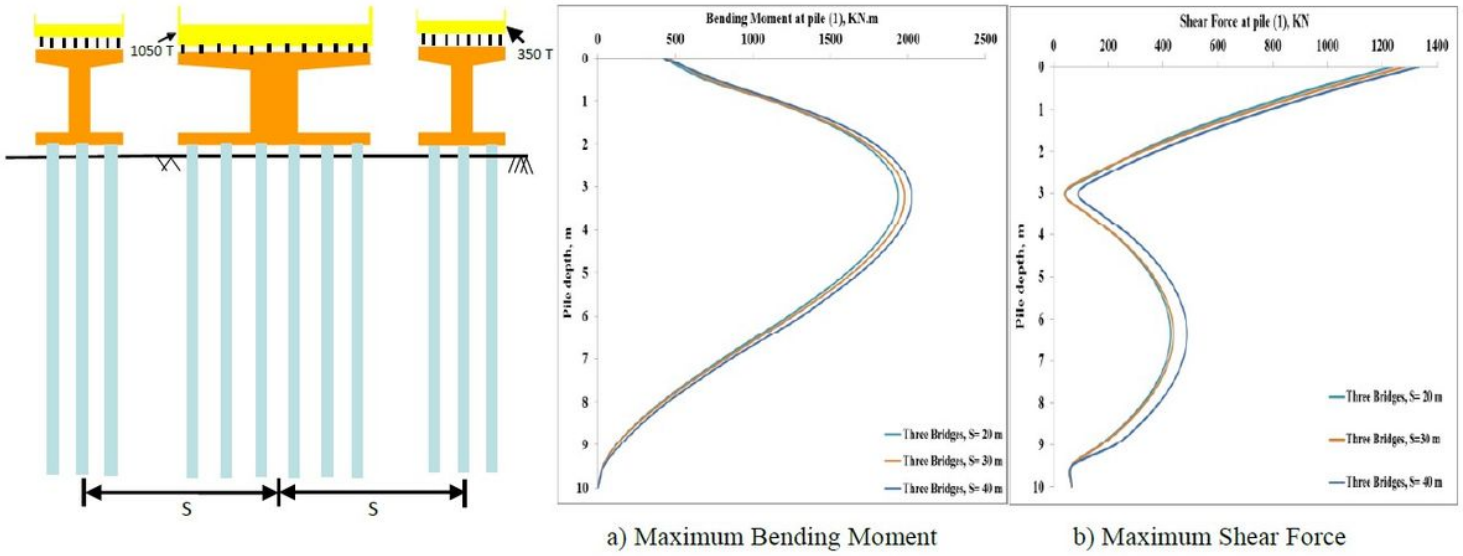

Figure 34

Three dissimilar parallel bridges: Internal forces at corner pile (1) of Bridge (350 T).

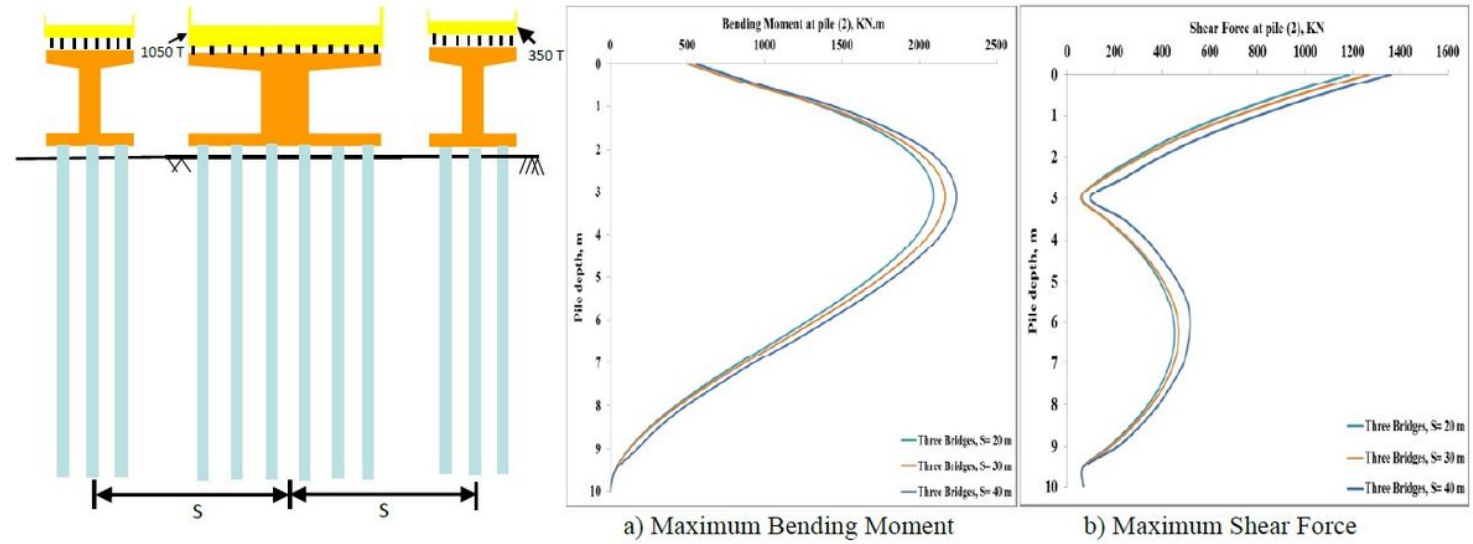

Figure 35

Three dissimilar parallel bridges: Internal forces at central pile (2) of Bridge (350 T).

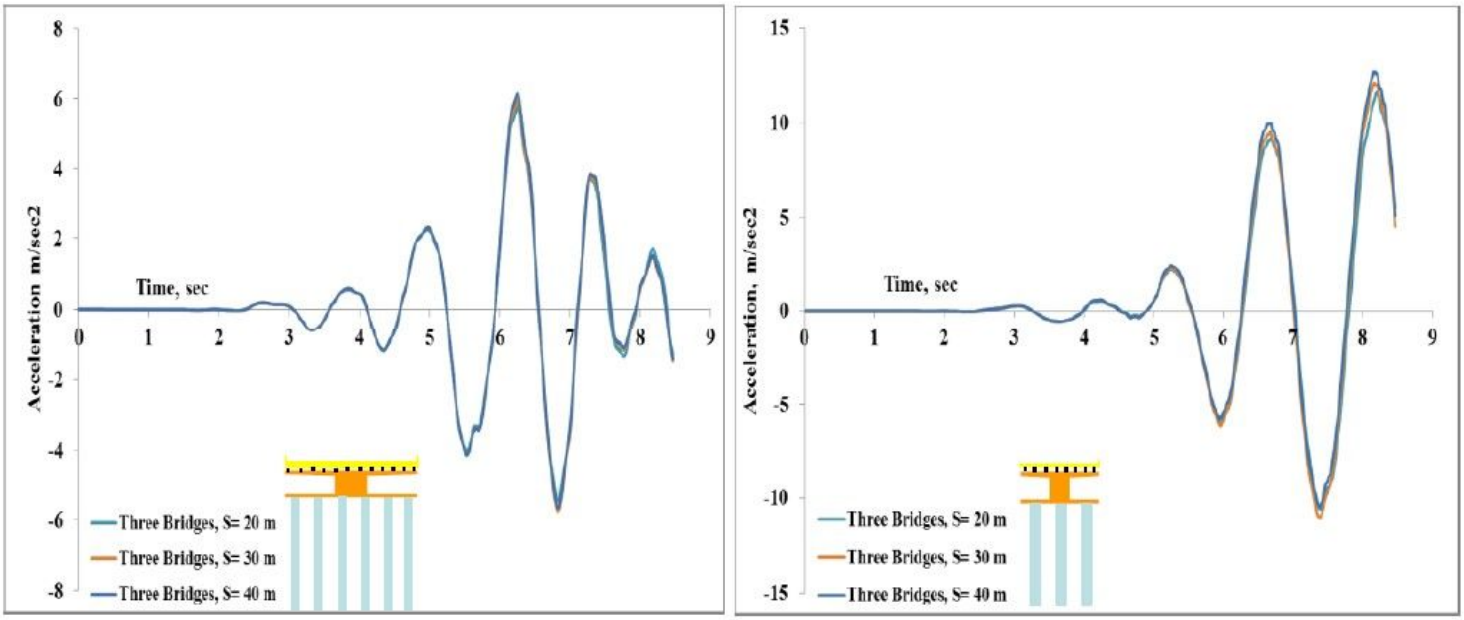

a) Mass (1050 T) Acceleration b) Mass (350 T) Acceleration

Figure 36

Three dissimilar parallel bridges: Masses Accelerations.

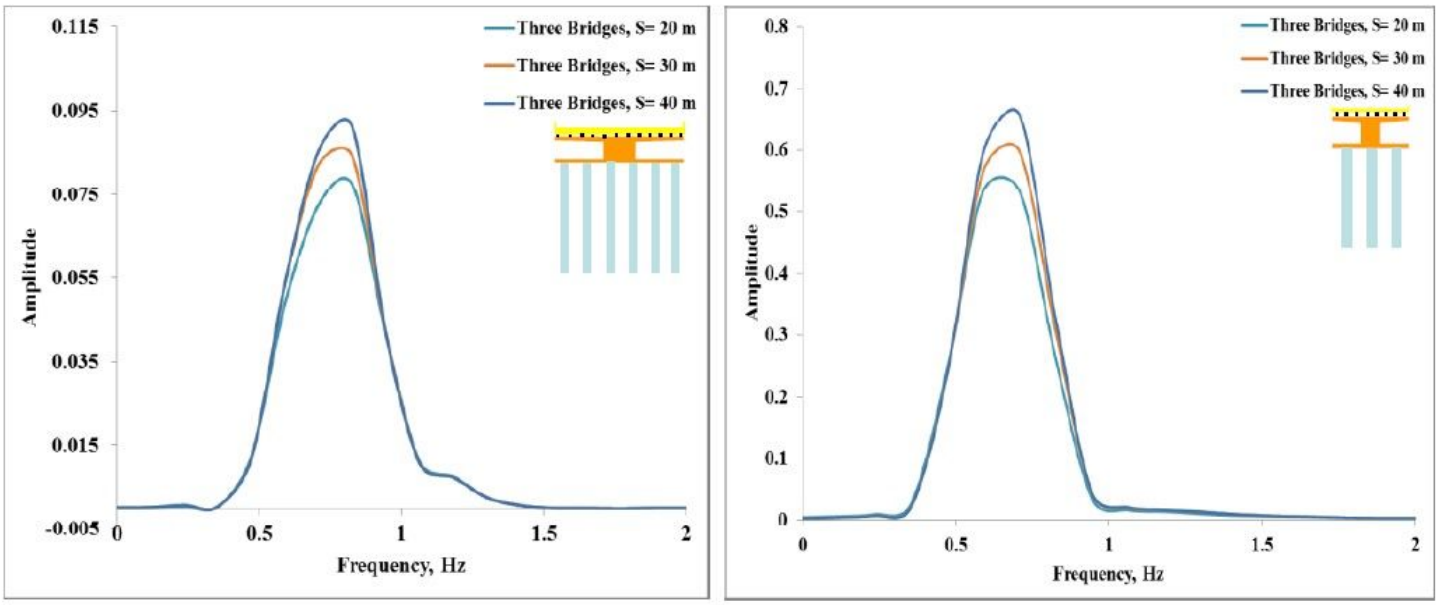

a) Mass (1050 T) b) Mass (350 T)

Figure 37

Three dissimilar parallel bridges: Fourier spectra diagram.

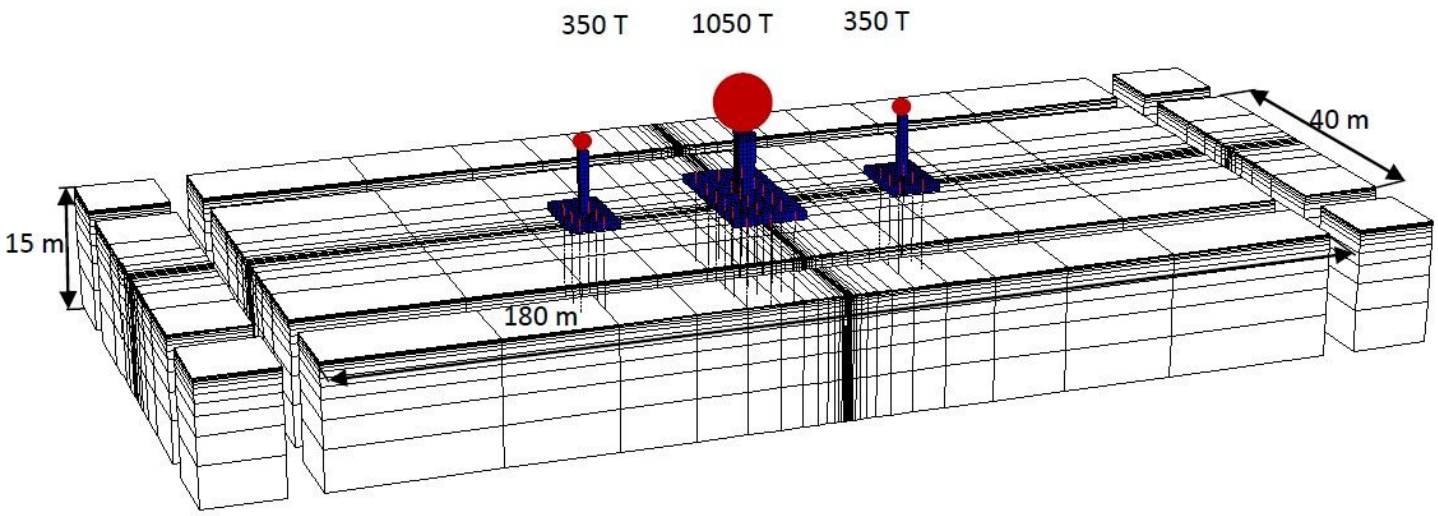

Figure 38

Bridge-Soil-Bridge System 3D numerical mesh with adsorbing boundaries (690 structural elements and 78286 nodes)

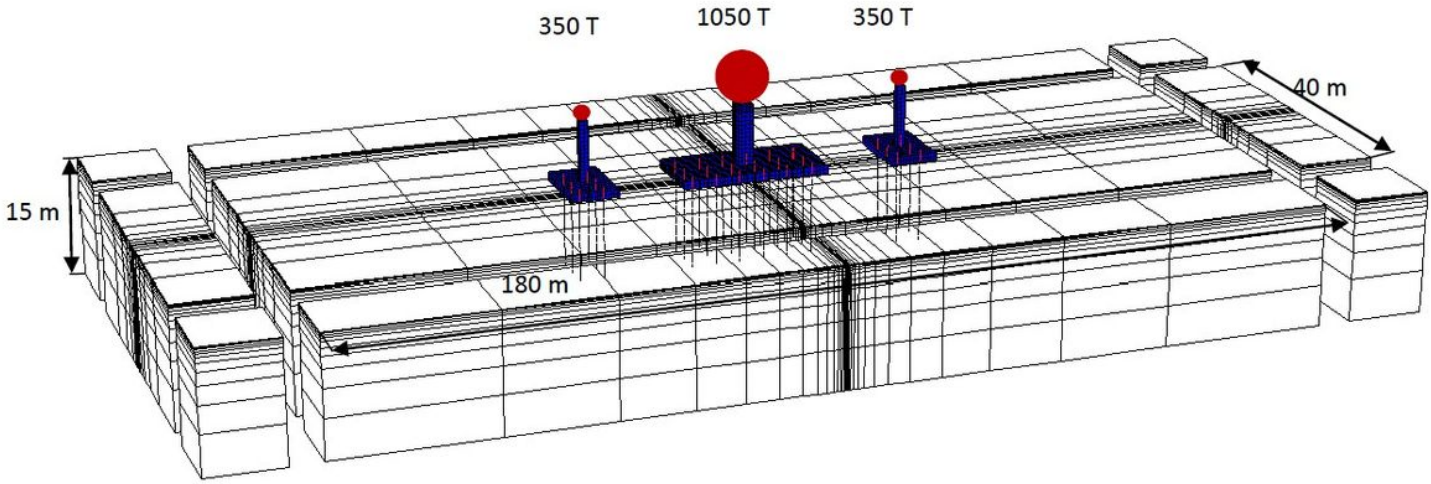

Figure 39

Bridge-Soil-Bridge System 3D numerical mesh with adsorbing boundaries (690 structural elements and 78286 nodes)

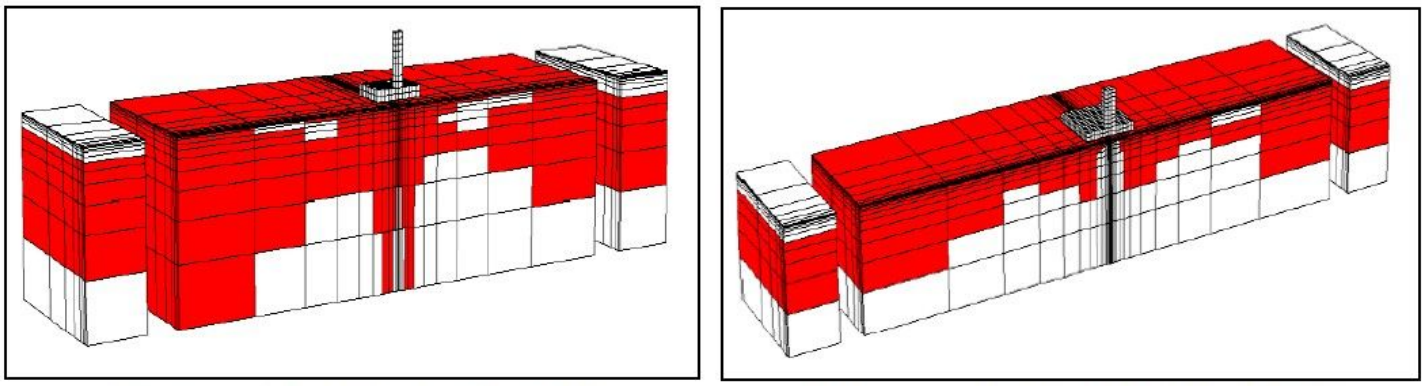

a) One perpendicular bridge (M_{st}=350 T)

b) One perpendicular bridge (M_{st}=1050 T)

Figure 40

Distribution of plasticity for two single isolated bridges (Mst=350 T) and (Mst=1050 T).

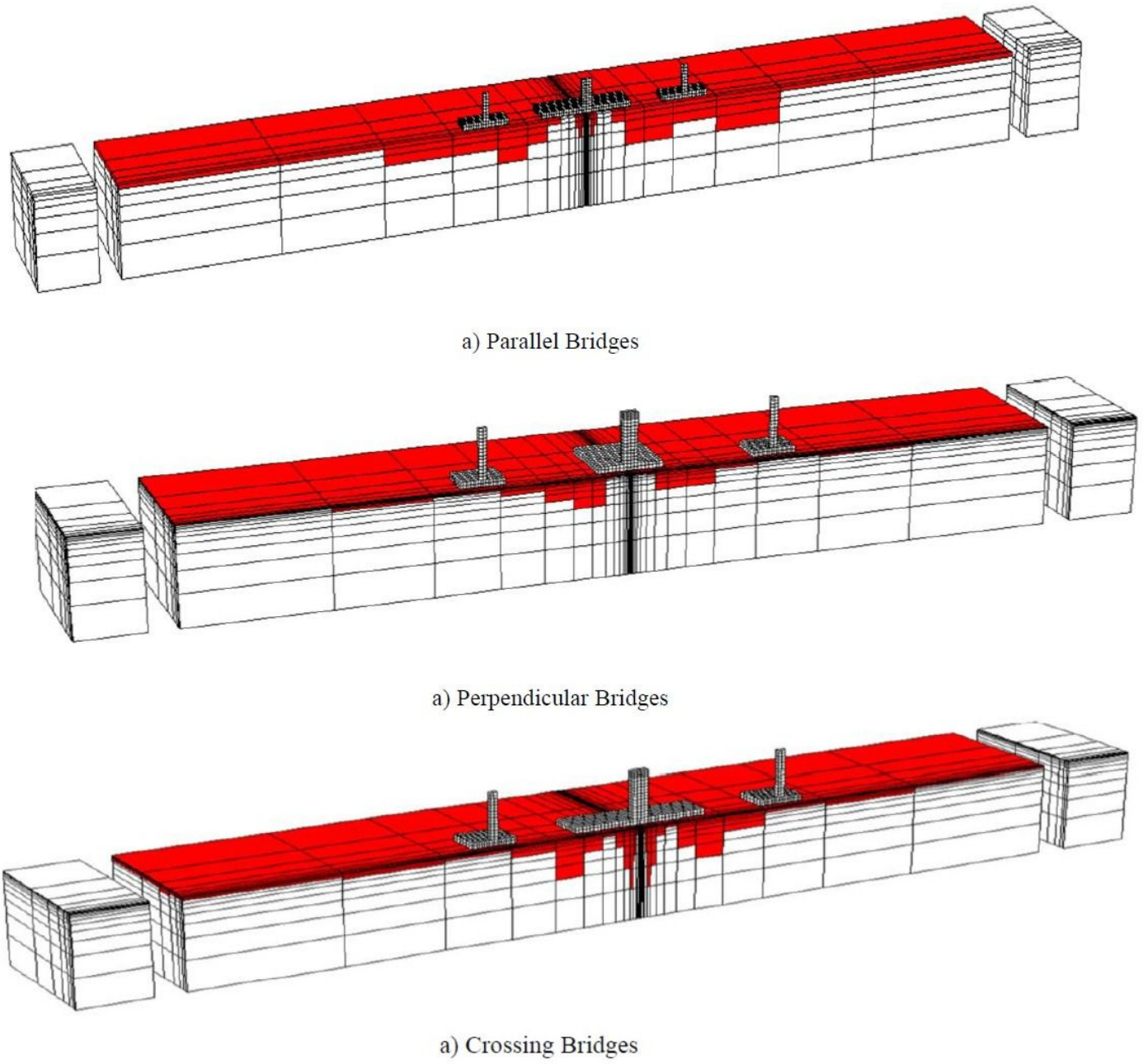

Figure 41

Distribution of plasticity (red zones) for different positioning of the three dissimilar Bridges. (Mst= 350 T, Mst= 1050 T, Mst= 350 T)

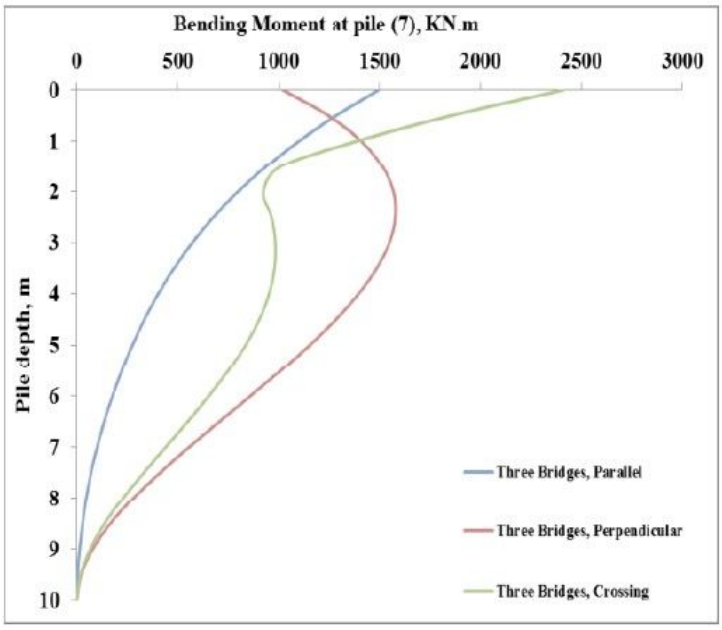

a) Maximum Bending Moment

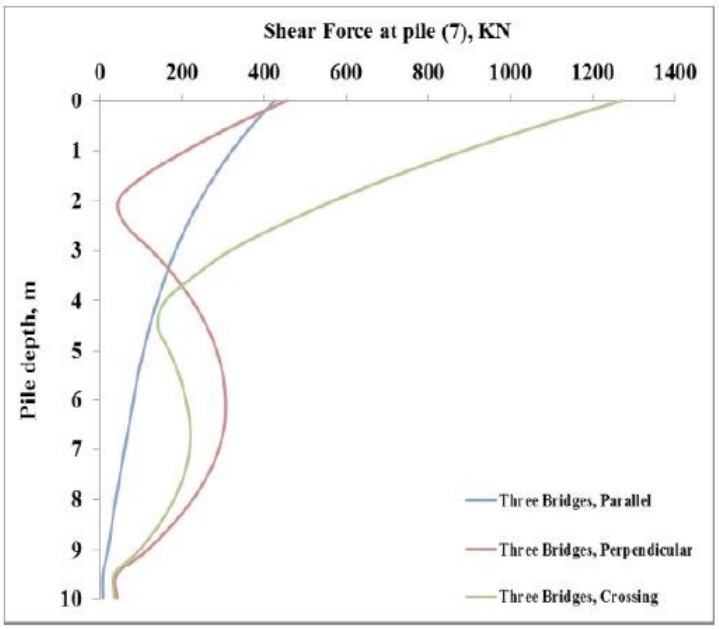

b) Maximum Shear Force

Figure 42

Three dissimilar bridges: Internal forces at corner pile (7) of Bridge (1050 T).

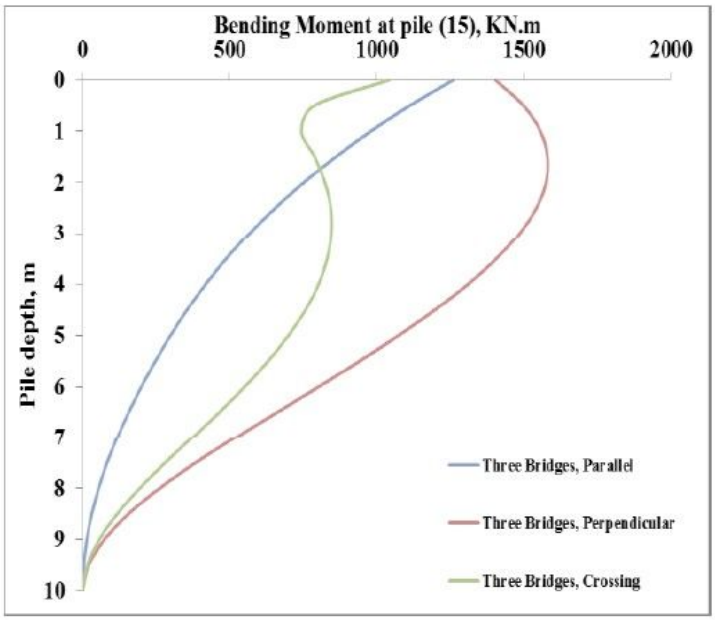

a) Maximum Bending Moment

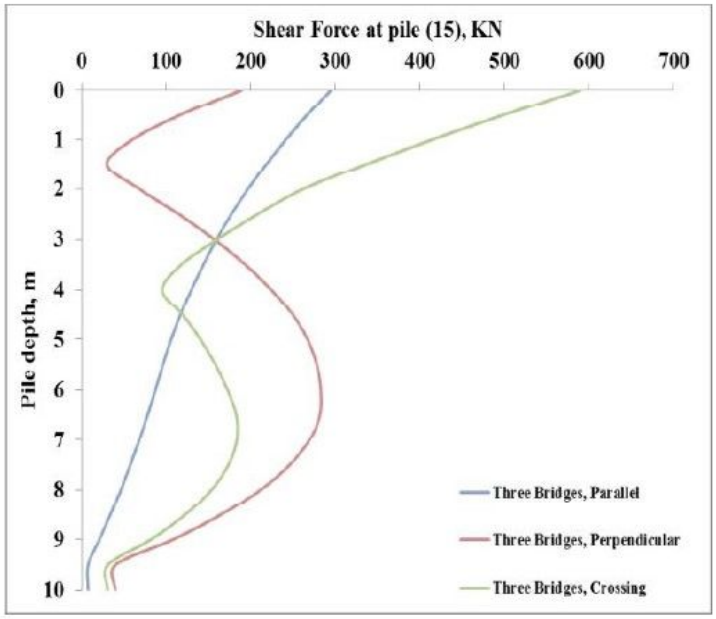

b) Maximum Shear Force

Figure 43

Three dissimilar bridges: Internal forces at central pile (15) of Bridge (1050 T).

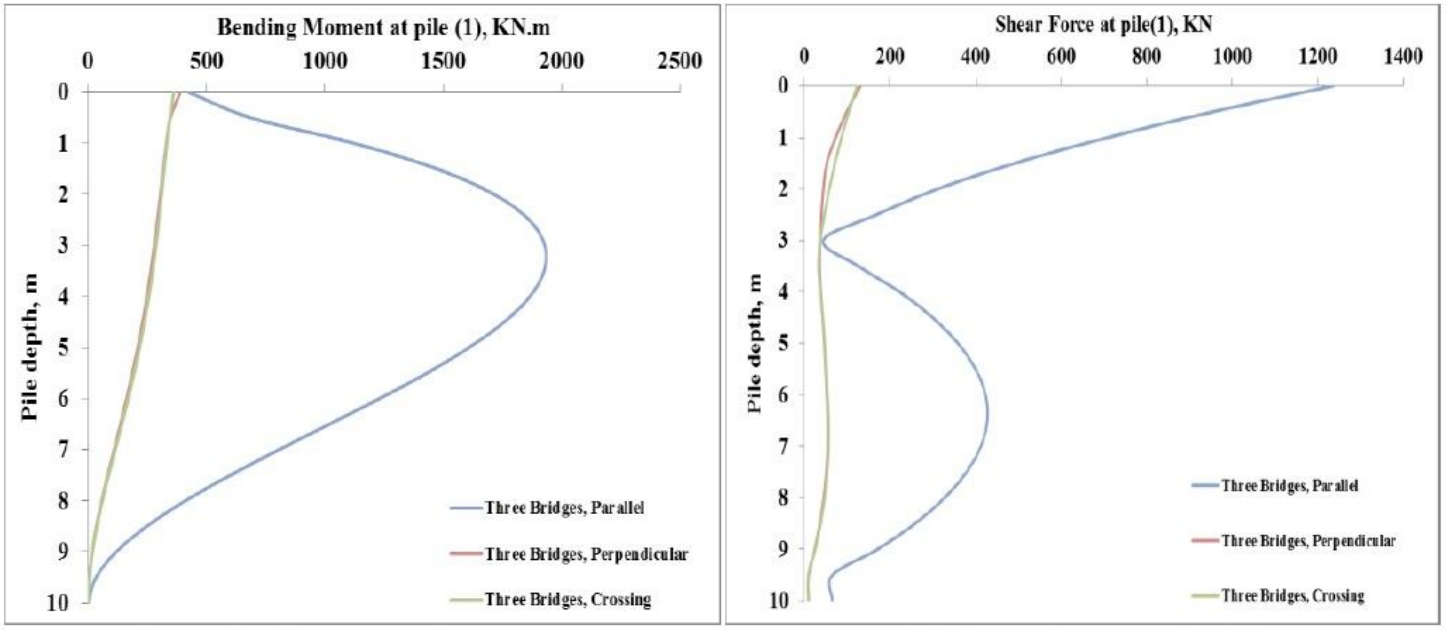

a) Maximum Bending Moment

b) Maximum Shear Force

Figure 44

Three dissimilar bridges: Internal forces at corner pile (1) of Bridge (350 T).

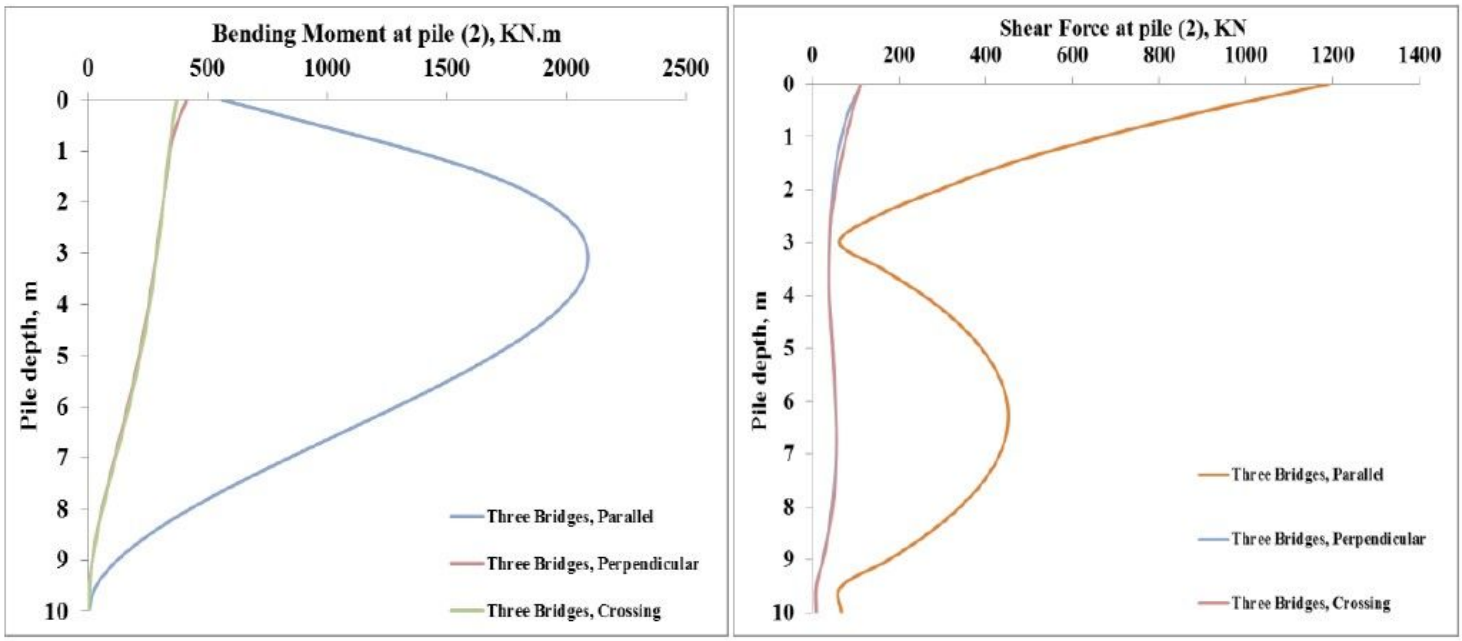

a) Maximum Bending Moment

b) Maximum Shear Force

Figure 45

Three dissimilar bridges: Internal forces at central pile (2) of Bridge (350 T).

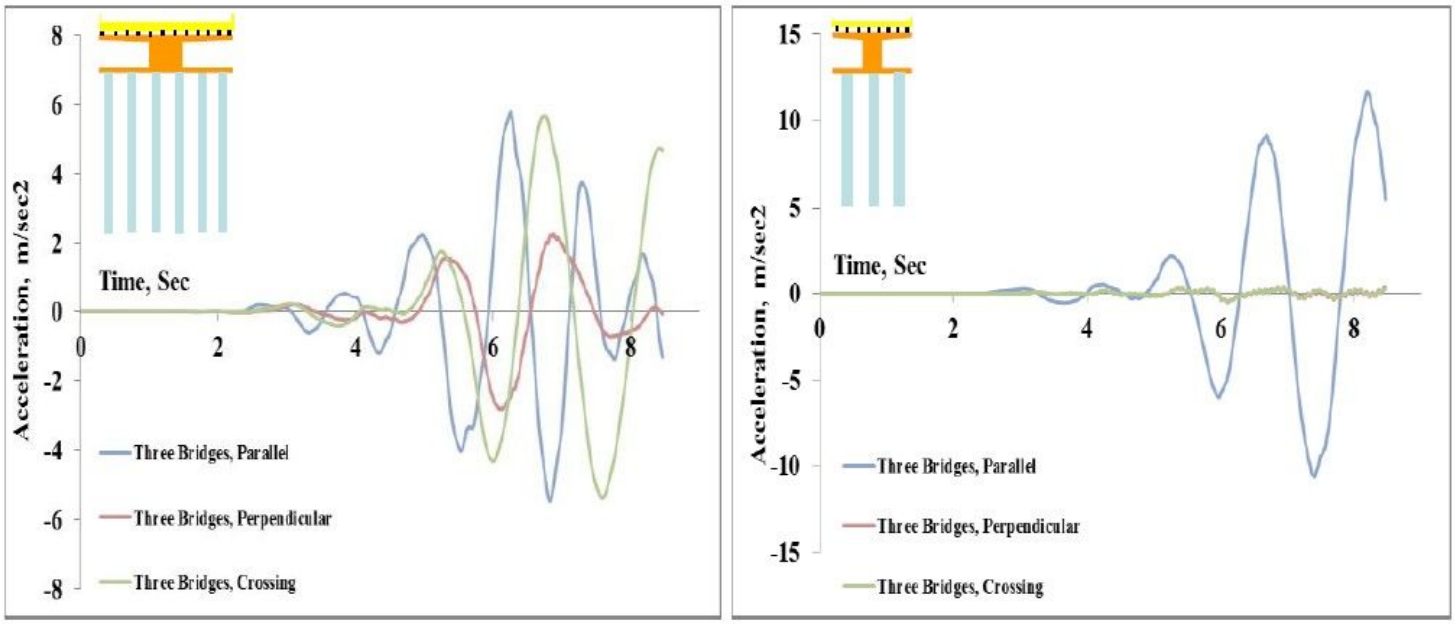

a) Mass (1050 T) Acceleration

b) Mass (350 T) Acceleration

Figure 46

Three dissimilar bridges: Masses Accelerations.

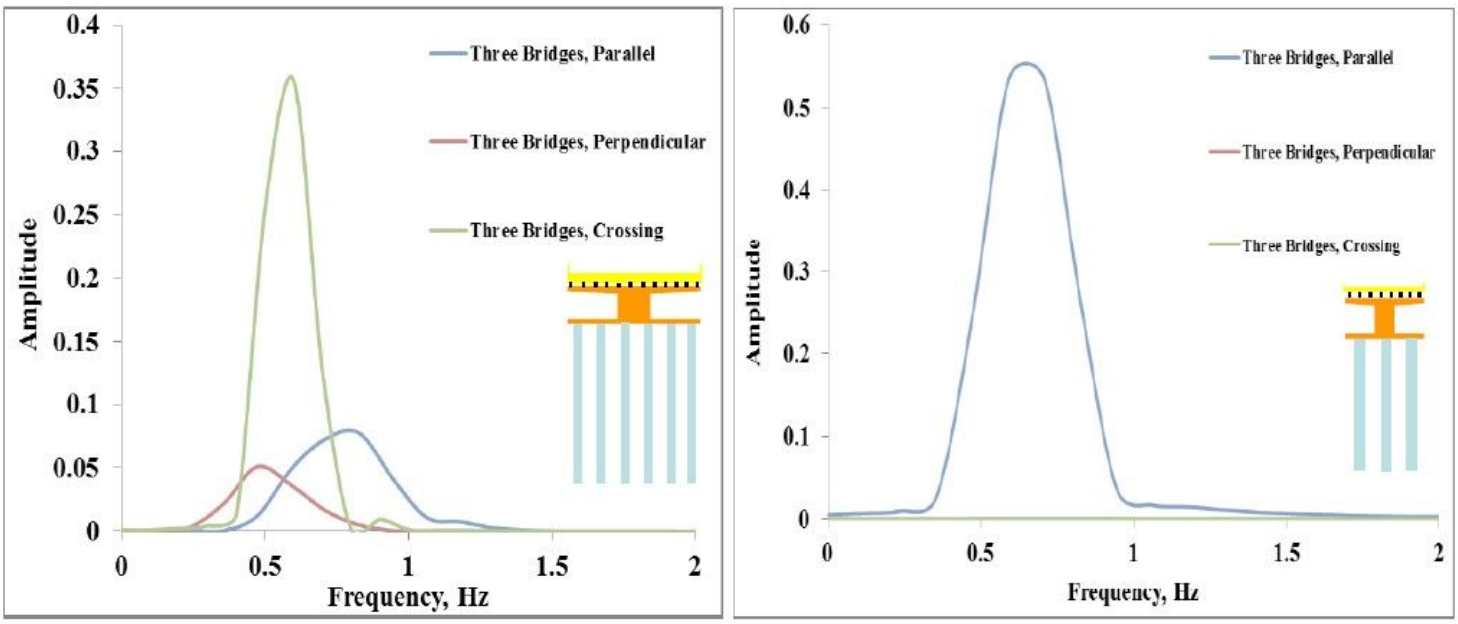

a) Mass (1050 T)

b) Mass (350 T)

Figure 47

Three dissimilar bridges: Fourier spectra diagram.